Excitation gaps in fractional quantum Hall states: An exact diagonalization study

R.H. Morf[(1)], N. d'Ambrumenil[(2)] and S. Das Sarma[(3)]
[(1)]*Condensed Matter Theory, Paul Scherrer Institute, CH-5232 Villigen, Switzerland*
[(2)]*Department of Physics, The University of Warwick, Coventry, CV4 7AL, UK*
[(3)]*Department of Physics, University of Maryland, College Park, MD 20742, USA*
(Dated: 22 February 2002)

We compute energy gaps for spin-polarized fractional quantum Hall states in the lowest Landau level at filling fractions $\nu = \frac{1}{3}$, $\frac{2}{5}$, $\frac{3}{7}$ and $\frac{4}{9}$ using exact diagonalization of systems with up to 16 particles and extrapolation to the infinite system-size limit. The gaps calculated for a pure Coulomb interaction and ignoring finite width effects, disorder and LL mixing agree well with the predictions of composite fermion theory provided the logarithmic corrections to the effective mass are included. This is in contrast with previous estimates, which, as we show, overestimated the gaps at ν =2/5 and 3/7 by around 15%. We also study the reduction of the gaps as a result of the non-zero width of the 2D layer. We show that these effects are accurately accounted for using either Gaussian or 'z$\times$ Gaussian' (zG) trial wavefunctions, which we show are significantly better variational wavefunctions than the Fang-Howard wavefunction. The Gaussian and zG wavefunctions give Haldane pseudopotential parameters which agree with those of self-consistent LDA calculations to better than $\pm$ 0.2%. For quantum well parameters typical of heterostructure samples, we find gap reductions of around 20%. The experimental gaps, after accounting heuristically for disorder, are still around 40% smaller than the computed gaps. However, for the case of tetracene layers in metal-insulator-semiconductor (MIS) devices we find that the measured activation gaps are close to those we compute. We discuss possible reasons why the difference between computed and measured activation gaps is larger in GaAs heterostructures than MIS devices. Finally, we present new calculations using systems with up to 18 electrons of the gap at $\nu = \frac{5}{2}$ including width corrections.

I. INTRODUCTION

Our understanding of the FQHE [1] is primarily based on the Laughlin wavefunction (wf) [2] and its appropriate hierarchical generalizations [3, 4, 5] for the so-called higher order "daughter" fractions which are many-electron wavefunctions in the lowest Landau level with no adjustable parameters. The fundamental property underlying the FQHE phenomenon is the existence, at certain filling fractions of the lowest Landau level, of an incompressible ground state and an energy gap Δ in the many-body excitation spectrum. This gap is produced entirely by the electron-electron interaction while the corresponding non-interacting single particle energy levels are all degenerate at the particular fractional filling (i.e. all non-interacting single particle levels have energy $\hbar\omega_c/2$ in the lowest Landau level, where $\omega_c = eB/(mc)$ is the cyclotron frequency in the magnetic field B).

The excitation gap Δ is the key measure of the robustness of the FQHE - the incompressibility cannot be destroyed by weak disorder in the system if the gap is large. The behavior of the gap as a function of filling fraction in the main sequence of FQHE states can also be compared to predictions of the composite fermion (CF) picture and used to extract the CF effective mass. The excitation gap at $\nu = 1/3$ has been theoretically estimated on the basis of exact diagonalization studies [6, 7] and Monte Carlo calculations [8, 9] as have the gaps at filling fractions $\nu = 2/5$ and $\nu = 3/7$ [10]. The numerically computed estimates of the gap are, however, significantly larger (by a factor of 2 to 3 at $\nu = 1/3$ for example) than the measured gaps, Δ_a, deduced from the activated temperature-dependence of the longitudinal resistivity minimum for each fraction [11, 12, 13, 14].

Here we report the results of extensive finite-size studies of the gap for spin-polarized excitations of electrons confined to the lowest Landau level (LLL) at filling fractions $\nu = \frac{1}{3}$, $\frac{2}{5}$, $\frac{3}{7}$ and $\frac{4}{9}$ as well as detailed results for the quantum Hall state at $\nu = \frac{5}{2}$. We give a detailed analysis of the finite size corrections and show that previous estimates of the gap [10] for the pure Coulomb interaction at $\nu = 2/5$ and $3/7$ were around 20% too high as a result of inaccurate extrapolation methods. For the simple exactly solvable case of a single hole in a filled polarized lowest Landau level, we demonstrate how an optimized extrapolation scheme dramatically reduces errors in the estimate for the infinite system result. We compare our new, more accurate, results with the predictions of composite fermion theory [15, 16, 17]. We find that, whereas previous estimates were consistent with a CF effective mass which was independent of filling fraction, the new estimates are in better agreement with the CF theory which predicts a logarithmically divergent effective mass as a function of filling factor as $\nu = 1/2$ is approached [15, 16]. The new results are also closer to the estimates of the effective mass from another type of finite-size calculations at $\nu = 1/2$ [18].

Other previous larger estimates of the pure Coulomb gap [19] may also involve an inaccurate extrapolation to the infinite system limit, but as these results were obtained using CF trial wf's and Monte Carlo techniques we cannot say for certain where the origin of this difference lies. However, we mention that our calculated excitation gaps are lower by as much as 30% than those in [19], and some discrepancy exists even for the pure Coulomb interaction results at $\nu = 1/3$ where our extrapolation to the thermodynamic limit is most reliable.

We clarify to what extent the discrepancy between numerically computed gaps and those extracted from transport measurements can be attributed to finite-width effects. The large disagreement between experimental activation gaps Δ_a and the numerically computed gaps Δ_c has been an outstanding

problem in the subject since the first accurate measurement of activation gaps was reported more than fifteen years ago [14]. There have been several previous theoretical attempts to compute realistic estimates of the energy gap and to identify the source of the large discrepancy between Δ_c and Δ_a [20, 21, 22, 23, 24, 25]. These took account of the finite thickness correction (i.e. relaxing the pure $1/r$ Coulomb interaction approximation by including the softening introduced by the transverse width of the 2D layer), and of the Landau level mixing corrections [26, 27]. There have also been studies of the spin-reversed excitations which are the lowest lying excitations for small g-factors and small magnetic fields [9, 28, 29, 30].

There are reports in the literature [22] that the finite-width effects account for all the difference between measured and theoretically predicted gaps. Our results are at variance with this conclusion [22] and consequently also with the results of [23] which were based on incorrect results from [22]. The error in [23] was originally corrected in [24, 25]. We find on the basis of the largest finite-size diagonalizations to date and of a careful analysis of the finite-size corrections that the finite-width corrections account for at most half of the difference between the computed gaps and those observed in GaAs heterostructures. On the other hand the gaps observed recently in tetracene in metal insulator semiconductor structures are only slightly smaller than our estimates. We discuss the possible reasons for these discrepancies. We argue that they are unlikely to be due to spin-reversed excitations or Landau-level mixing and suggest that they are the result of disorder effects which may affect the activation energy for transport differently in heterostructures and MIS devices.

We show that it is unlikely for there to be a transition from an incompressible to a compressible state at fixed filling factor, for $\nu = \frac{1}{3}, \frac{2}{5}, \frac{3}{7}$, caused by a gap collapse induced entirely by the softening of the Coulomb interaction due to the finite thickness corrections. Such a transition has been conjectured to occur in the second Landau level [31, 32], where the FQHE is much less robust. It may also happen in situations where increasing the width in the transverse direction changes the symmetry of the sub-band wf [33]. Alternatively, a new kind of FQH state can arise in square, parabolic or double wells, where, for large enough well width, the wf may split into an effective double layer structure at the two ends of the well with a central self-consistent barrier separating these two effective layers [34]. In the regular GaAs heterostructure system [11, 12, 13, 14] we find the lowest Landau level $\nu = \frac{1}{3}, \frac{2}{5}, \frac{3}{7}$ FQHE to be robust with respect to the finite thickness effect, with $\Delta > 0$ even for the largest possible (and physically allowed) transverse thickness. However the actual value of Δ may become rather small and one might have to go to very low temperatures (and very high quality, low disorder samples) to observe the FQHE. Our results are in conflict with the claim by Park et al. [23, 25, 35] that the finite width alone can lead to the loss of incompressibility at a filling fraction $\nu = p/(2p+1)$ for some finite value $p = p_c$.

We also compare the various approximate methods for accounting for finite thickness effects based on interfacial trial wf's with those taken from self-consistent local density approximation (SCLDA) calculations [22, 36]. Previous model calculations have used Gaussian and Fang-Howard envelope wf's and the Zhang-DasSarma (ZDS) model interaction [20]. We introduce a new variational envelope wf, the "z $\times$Gaussian" (zG). We find that both the zG and the Gaussian envelope wf's give Haldane pseudopotential parameters which agree to within fractions of a percent with those from the full SCLDA wf's with the zG giving slightly more accurate results at the densities used in experiment. However, both give essentially indistinguishable results for excitation energies and gaps from those taken from the SCLDA wf's. This result shows that accurate finite-size studies of finite-width effects require only the determination of the appropriate width parameter in either the Gaussian or zG description and do not require the use of SCLDA based tables of parameters [22].

We show that depending on the sub-band density either the Gaussian or zG variational wf provide substantial quantitative improvements over the well-known Fang-Howard variational wf [37] which has been employed extensively in heterostructure electronic calculations. Indeed, it turns out that the Fang-Howard wf generally overestimates the kinetic energy, and consequently predicts significantly too large width. The expectation value of the energy and other quantities of interest in this context can be calculated analytically for these variational wf's, and in the case of the Gaussian, it is easy to perform expansions for either very small or very large width. Finally in the Appendix, we explain why the ZDS model is not reliable directly for predicting finite thickness corrections, but we present a simple modification which corrects its main shortcoming.

The remainder of this paper is organized as follows: In section II we describe the diagonalization of the N-particle Hamiltonian in the spherical geometry and give the definitions of the quasiparticle, quasihole and gap energies. In section III, we discuss the extrapolation to the $N \to \infty$ limit and in section IV we compare the variation of the calculated gaps with filling fraction ν with the predictions of composite fermion theory [15, 16, 17]. In section V we show how variational wf's can be used to model finite width effects. In section VI, we compute the reduction of the energy gaps as a function of the finite width and in section VII we compare our results for the gap energies with experimentally reported estimates of gaps.

II. QUASIPARTICLE AND QUASIHOLE ENERGIES

We model the two-dimensional electron gas using Haldane's spherical geometry [3]. Particles with coordinates (R, θ_i, ϕ_i) move in a monopolar magnetic field of strength $B = S\hbar/eR^2$ which gives rise to $2S+1$ linearly independent cyclotron orbits in the lowest Landau level. The single particle orbitals on the surface of the sphere for the particles in the lowest Landau level are then functions $\psi(\theta_i, \phi_i)$ which are the lowest energy eigen states of the kinetic energy.

In the lowest Landau level, the interaction between particles

is written

$$V(ij) = \sum_m \sum_{i<j}^{N} V_m P_m(ij) \tag{1}$$

where $P_m(ij)$ projects onto states in which particles i and j have relative angular momentum $m\hbar$ and V_m gives their interaction energy for this relative angular momentum. The set V_m, called Haldane pseudopotentials [3], completely characterizes the interaction between particles confined to the lowest Landau level. In terms of the electron-electron interaction, $V(r)$, they are defined in the plane by [38]

$$V_m^{(n)} = \frac{1}{(2\pi)^2} \int d\vec{r} V(r) \int d\vec{q} e^{i\vec{q}.\vec{r} - (q\ell_0)^2} \left(L_n(\frac{q^2\ell_0^2}{2}) \right)^2 L_m(q^2\ell_0^2), \tag{2}$$

where n refers to the Landau level and $V(r)$ stands for the electron electron interaction. The corresponding integrals for electrons on the surface of a sphere are described in [6]. In the lowest Landau level $n = 0$, the first Laguerre polynomial in equation (2) is equal to unity. As we shall discuss in the next section, the effect of the finite width of the wf, $\phi(R_i)$, is incorporated in these pseudopotential parameters $V_m^{(n)}$. In the following, we will drop the superscript $n = 0$ and denote the Haldane pseudopotentials for the lowest Landau level by V_m.

The method for computing excitation energies and gaps in this geometry has been described in detail in many places [3, 7, 10]. According to the hierarchy model, the FQHE ground states at filling fraction ν occur for a system of N particles when the total flux $2S$ is given by

$$2S_0(\nu, N) = \nu^{-1} N + X(\nu) \tag{3}$$

where $X(\nu)$ is the shift function [10], which is a characteristic of the geometry of the system (in this case the sphere) [39]. Laughlin's [2] elementary fractionally charged excitations from the FQHE ground state at filling fraction $\nu = p/(2p+1)$ correspond to the ground state configuration of a system with additional/missing flux $\pm 1/p$,

$$2S_{\pm 1/p}(\nu, N) = 2S_0(\nu, N) \pm \frac{1}{p}. \tag{4}$$

At $\nu = 1/m$ there are systems with both $2S_0$ and $2S_{\pm 1/p}$ both integer for all integer N. At other filling fractions $2S_0$ and $2S_{\pm 1/p}$ are never both integer for the same N. For example at $\nu = 3/7$, $2S_0$ is integer when the particle number is $N = 3n$ (n integer) while $2S_{\pm 1/3}$ is integer for $N = 3n \mp 1$, respectively. We take the energy to nucleate a single quasiparticle/quasihole in a system of N particles at filling fraction ν, $e_\nu^{\pm}(N)$, to be the total energy difference between the lowest energy state with total flux $2S_{\pm 1/p}(\nu, N)$ and the total ground state energy the system would have at $2S_0(\nu, N)$ for the same N, i.e.

$$e_\nu^{\pm}(N) = E_{2S_{\pm 1/p}}(N) - E_{2S_0}(N). \tag{5}$$

Here $E_{2S\pm 1/p}(N)$ is the total energy of the system of N particles in their ground state in $2S_{\pm 1/p}$ flux quanta. For filling fractions $\nu = 1/m$ we can calculate both energies directly,

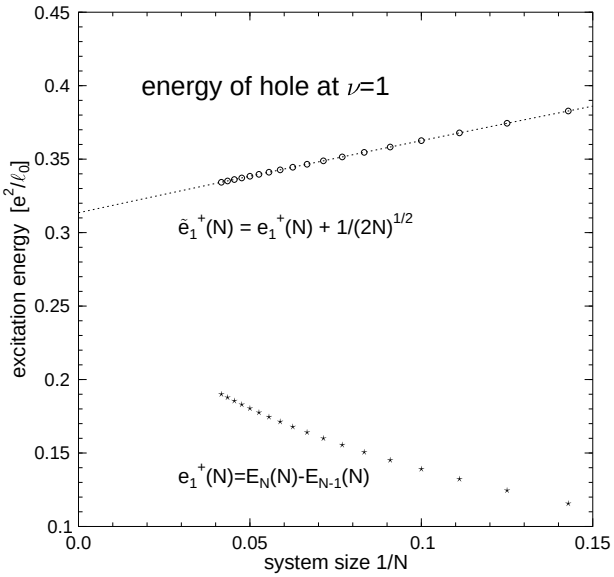

Figure 1: The energy of a single hole. The asterisks show $e_1^+(N)$ and the circles show the corrected energy $\tilde{e}_1^+(N)$. The extrapolation in $1/N$ of the corrected energies pass through the exact value $\frac{1}{4}\sqrt{\pi/2}$ whereas extrapolation of $\varepsilon_1^+(N)$ in $1/N$ would give incorrect results.

while at filling fractions $\nu = p/(2p+1)$ with $p \neq 1$ we have to estimate $E_{2S_0}(N)$ by interpolating (or extrapolating for the largest system sizes) between system sizes for which we can compute $E_{2S_0}(N)$.

III. ENERGY GAPS: FINITE SIZE EFFECTS AND THE THERMODYNAMIC LIMIT

From studying the variation with system size of the energies to nucleate quasiparticles and quasiholes in finite-size systems we estimate the excitation energies in the thermodynamic limit. It is essential that the extrapolation procedure is carried out carefully. Firstly, if working with the Coulomb interaction it is usual to quote energies in units of $e^2/\varepsilon\ell_0'$, where $\ell_0' = \sqrt{\hbar c/eB}$ is the magnetic length and ε is the dielectric constant for the medium. However, for systems with number density n_S on the sphere, $\ell_0' = \sqrt{(1/(2\pi n_S))(N/(2S))}$ and so for systems at fixed density, the magnetic length ℓ_0' depends on the particle number and the total flux through the ratio $N/2S$. In order to compare quantities measured in the same units we convert all energies by using the magnetic length in the infinite system $\ell_0 = \sqrt{\nu/(2\pi n_S)}$.

There is also a systematic contribution to the excitation energy in a finite size system which scales to zero in the thermodynamic limit, which we can take account of explicitly [10]. When the localized quasiparticle/quasihole excitation which is formed in a system of N particles around the point on the sphere $R\vec{\Omega}$ with $\vec{\Omega}$ a unit vector pointing away from the origin a charge $\pm qe$ with $q = 1/(2p+1)$ is concentrated around this point. This charge has come from the rest of the system. There is then a contribution, A_q, to the energy of the system

from the non-uniform distribution of charge on the surface of the sphere which, in units of $e^2/\varepsilon\ell_0$, is given by

$$A_q(\nu) = -q^2\sqrt{\frac{\nu}{2N}}. \quad (6)$$

To extrapolate to the infinite system size limit it is better to remove this contribution explicitly and study the corrected quasihole and quasiparticle energies

$$\widetilde{e}^{\pm}_{\nu}(N) \equiv e^{\pm}_{\nu}(N) - A_q(\nu). \quad (7)$$

We also define the corrected gap energies to be the sum of quasiparticle and quasihole energies

$$\widetilde{e}^{g}_{\nu}(N) \equiv \widetilde{e}^{+}_{\nu}(N) + \widetilde{e}^{-}_{\nu}(N). \quad (8)$$

We denote the limit $N \to \infty$ of the gap and quasihole, quasiparticle excitation energies by $\widetilde{\varepsilon}^{(g)}_{\nu}$ and $\widetilde{\varepsilon}^{\pm}_{\nu}$ respectively.

To illustrate the importance of working with these corrected energies, we show results for a single hole at $\nu = 1$, which is a case for which the energy can be computed analytically using the exact expression for the energy of a filled Landau level [40]. We find

$$e^{+}_{1}(N) = -\frac{1}{2}\frac{E_{N-1}(N)}{N}\left(1+\frac{3}{2N+1}\right) - \frac{1}{\sqrt{2N}}. \quad (9)$$

The contribution $-1/\sqrt{2N}$ is just the correction $A_1(1)$ for the case $\nu = 1$. Both $e^{+}_{1}(N)$ and $\widetilde{e}^{+}_{1}(N)$ are shown as a function $1/N$ in Figure 1. It is clear from the figure that extrapolation of $e^{+}_{1}(N)$ with $1/N$ would give spurious results because of the contribution of $A_1(1)$, which varies as $1/\sqrt{N}$. By contrast, extrapolation of $\widetilde{e}^{+}_{1}(N)$ with $1/N$ gives the correct result [41] $\lim_{N\to\infty}(-E_{N-1}(N)/(2N)) = \frac{1}{4}\sqrt{\pi/2}$.

In Figure 2 we show $\widetilde{e}^{+}_{1/3}(N)$ and $\widetilde{e}^{-}_{1/3}(N)$ and their extrapolations to $N = \infty$ using least squares fits to linear and quadratic functions in $1/N$. We take the difference, 0.0005 for the quasiparticle and 0.0002 for the quasihole, in the estimates from the two different extrapolation procedures as our measures of the accuracy of the extrapolation. In fact, inclusion of the $1/N^2$ term in the fit does not improve the χ^2 value significantly. So, in the following, we will always use linear extrapolation in $1/N$ to compute gaps in the thermodynamic limit. Figure 3 shows the gap energies at $\nu = 1/3$ and $2/5$ as functions of $1/N$ and the extrapolations to $N = \infty$ limit together with the estimates based on the study of trial CF-wf's [19]. Plotted are the sum of quasiparticle and quasihole energies $\tilde{e}^{-}(N) + \tilde{e}^{+}(N)$, using the correction $A_q(\nu)$ (6) and the energy $\tilde{e}_{exc}(\nu)$ of the neutral excitation with $L = L_{max}$ (cf. caption to Figure 3), corresponding to maximum separation of the quasiparticle and quasihole on the sphere, again corrected by the term $A_q(\nu)$ which stands for the Coulomb energy between the quasiparticle and quasihole. As can be seen, the size dependence of the exciton energies is much less smooth than that of the sum of qp- and qh-energies. Indeed, if they were known only for small systems, extrapolation to the bulk limit would be inaccurate. Only for the largest systems, does the size dependence

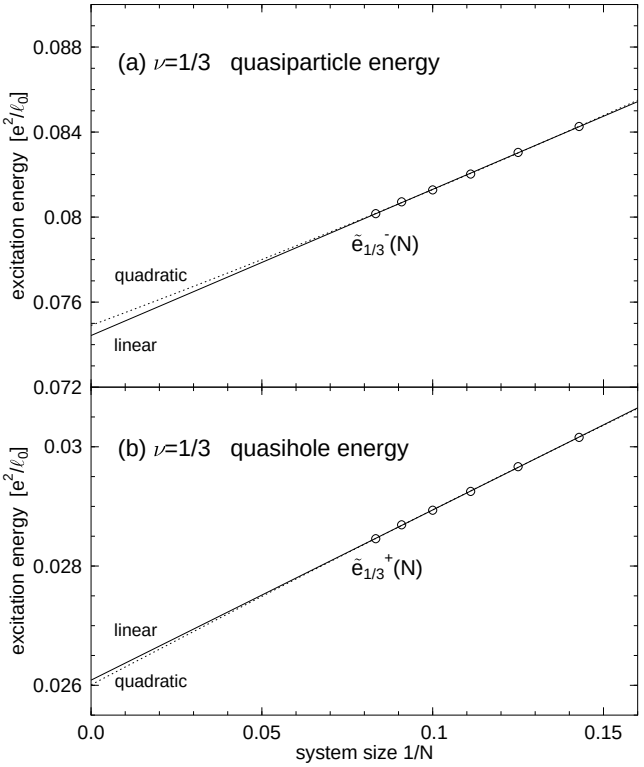

Figure 2: The quasiparticle ($\widetilde{e}^{-}_{1/3}(N)$) and quasihole ($\widetilde{e}^{+}_{1/3}(N)$) energies at $\nu = 1/3$ and the extrapolation using linear and quadratic functions of $1/N$. We take the small differences in the extrapolated result as a measure of the accuracy of the extrapolation.

of exciton energies become smooth and allow reliable extrapolation to the thermodynamic limit, which is consistent with that based on the sum of qp- and qh-energies, although less accurate (see Figure 3).

Figure 4 shows the quasiparticle and quasihole energies at $\nu = 3/7$ and $4/9$. Although the estimate at $\nu = 1/3$ is close to the values quoted previously [10], the values at $\nu = 2/5$ and $3/7$ are around 20% smaller although still within the large uncertainties of the earlier calculation. Our latest estimates are more accurate as a consequence of a better understanding of finite size effects in addition to being able to diagonalize the Hamiltonians for larger systems (with up to around 100 million basis states) - 15 particles instead of 11 particles for the quasiparticle and quasihole at $\nu = 2/5$ and 16 particles instead of 13 for the quasiparticle at $\nu = 3/7$. It is interesting to note that the extrapolation of quasiparticle and quasihole energies at $\nu = 1/3$ based on small sizes ($N = 4, 5, 6$) yields the values $\tilde{\varepsilon}^{-}_{1/3} \approx 0.0757$, $\tilde{\varepsilon}^{+}_{1/3} \approx 0.0267$ and for the gap $\Delta_{1/3} \approx 0.1024$. These are within about one percent of our best estimates of the bulk limit of $\tilde{\varepsilon}^{-}_{1/3} = 0.0749$, $\tilde{\varepsilon}^{+}_{1/3} = 0.0263$ and for the gap $\Delta_{1/3} = 0.1012$, obtained using system sizes up to $N = 12$ and performing the extrapolation by linear polynomial fit in $1/N$. Likewise at $\nu = 2/5$, extrapolation using the results at $N = 5, 7, 9$ yields values for the bulk limit for the quasiparticle and quasihole energies of $\tilde{\varepsilon}^{-}_{2/5} \approx 0.0431$ and $\tilde{\varepsilon}^{+}_{2/5} \approx 0.00920$ and a value for the gap $\Delta_{2/5} \approx 0.0523$, while our best esti-

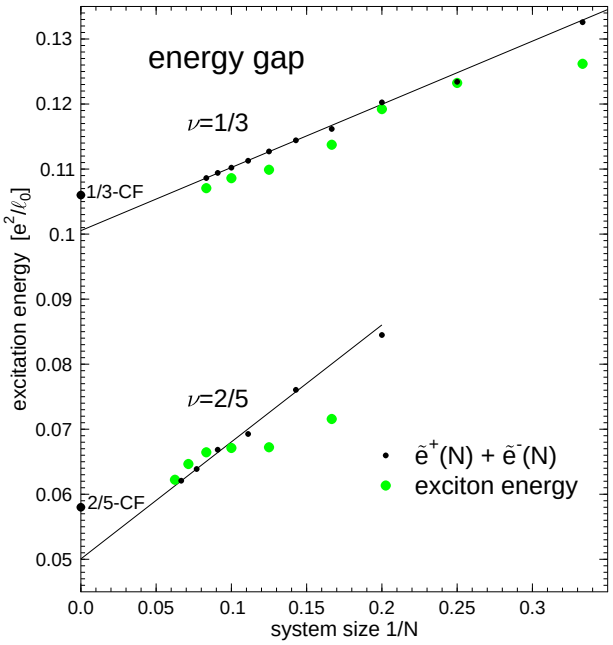

Figure 3: The gap energies $\tilde{e}^g_\nu(N)$ at $\nu = 1/3$ and $2/5$, computed using (8) (small solid dots), and the neutral exciton energies for $L = N$ at $\nu = 1/3$ and $L = (N+2)/2$ at $\nu = 2/5$ (large shaded dots). Also shown by circles on the vertical axes are the estimates of the gap energies of Jain and Kamilla [19] obtained from an analysis of trial composite fermion wf's. The straight lines denote the best linear (in $1/N$) fit to the data points. The intercepts give the estimate of the gap energy $\tilde{e}^g_\nu(\infty)$ neglecting corrections due to non-zero width effects and higher Landau levels.

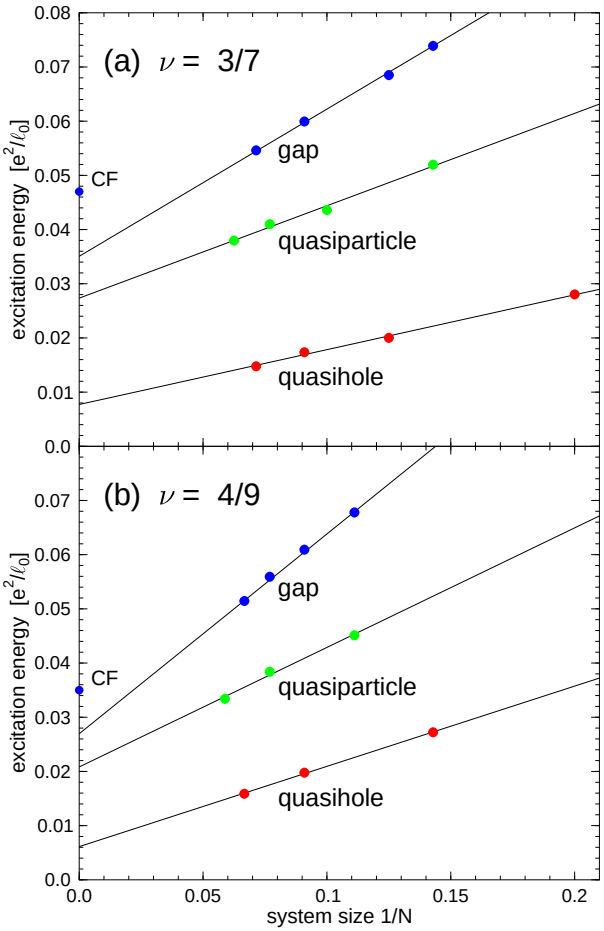

Figure 4: The quasiparticle and quasihole energies $\tilde{e}^\pm_\nu(N)$ at $\nu = 3/7$ and $4/9$ and the best linear fits to these points. The sum of the two linear functions can be taken as a measure of the gap energies $\tilde{e}^g_\nu(N)$ (these cannot be computed directly for these filling fractions as the systems with single quasiparticle and quasiholes have different numbers of particles).

mate based on system sizes $7 \le N \le 15$ are $\tilde{\varepsilon}^-_{2/5} = 0.0398$, $\tilde{\varepsilon}^+_{2/5} = 0.0102$ and the gap $\Delta_{2/5} = 0.0500$, corresponding to a difference for the gap of about 5 percent. This observation makes us confident that it is now also possible to compute reliable bulk limit values for the gaps at $\nu = 3/7$ and $4/9$. Our values are $\Delta_{3/7} = 0.035$ and $\Delta_{4/9} = 0.027$. The systems at $\nu = 4/9$ were inaccessible in our earlier work [10].

IV. EFFECTIVE MASS OF COMPOSITE FERMIONS

Our estimates of the gap energies in the sequence of states $\nu = p/(2p+1)$ are compared in Figure 11 with the predictions of CF theory [15, 16, 17], which for this sequence gives (in units of $e^2/\varepsilon\ell_0$)

$$\tilde{\varepsilon}^g_\nu \equiv \tilde{e}^g_\nu(\infty) = \frac{\pi}{2}\frac{1}{|2p+1|\,(\ln|2p+1| + C')}. \qquad (10)$$

Choosing $C' = 4.11$ to fit the gap at $\nu = 1/3$ gives the gaps at $\nu = 2/5$, $3/7$ and $4/9$ to be 0.0549, 0.0371 and 0.0276 which are remarkably close to the estimates we obtain. We also note that, whereas the earlier estimates were better fitted by assuming that the gaps were simply proportional to $1/(2p+1)$ (i.e. ignoring the logarithmic corrections), Figure 5 shows that the new results are better described by the theory when the logarithmic corrections to the gap are included. This translates into an effective mass

$$m^*(p) = \hbar^2 \left(\frac{\varepsilon}{e^2\ell_0}\right) F(p) \qquad (11)$$

where

$$F(p) = \frac{2}{\pi}\left[\ln|2p+1| + 4.11\right]. \qquad (12)$$

The effective mass of CF's has also been estimated by studying the variation with system size of the ground state energy for systems of electrons close to $\nu = 1/2$ on the sphere with $2S_0(1/2, N) = 2N - 2$ [18]. These studies gave $F \sim 5$, which is about 25% larger than the value we obtain for $p = 4$. One would expect that, in systems close to $\nu = 1/2$, the effective mass would be larger than at $\nu = 4/9$ but still finite as the long-wavelength fluctuations of the Chern-Simons gauge field, which give rise to the logarithmic divergence in the effective mass, will be cut off by the level spacing.

In [10] estimates of the gap energies based on collective excitations were also presented. On a sphere the effective

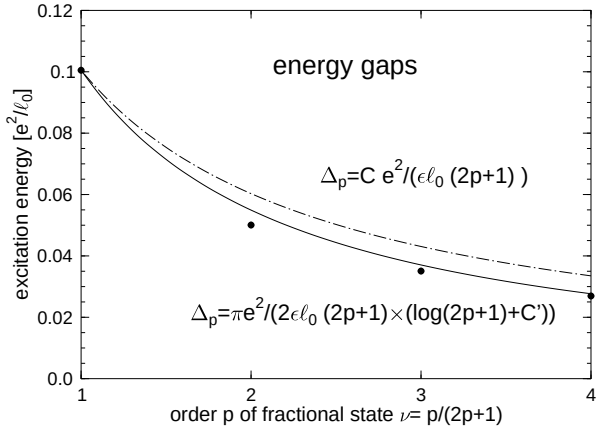

Figure 5: The gap energy as a function of level in the hierarchy, p. The estimates based on our finite-size studies of systems with $\nu = 1/3$, $2/5$, $3/7$ and $4/9$ are shown as dots. The lower (upper) curve shows the prediction of the CF theory with (without) and logarithmic corrections from (10). The constants C and C' are chosen to give the correct gap at $p = 1$ ($\nu = 1/3$).

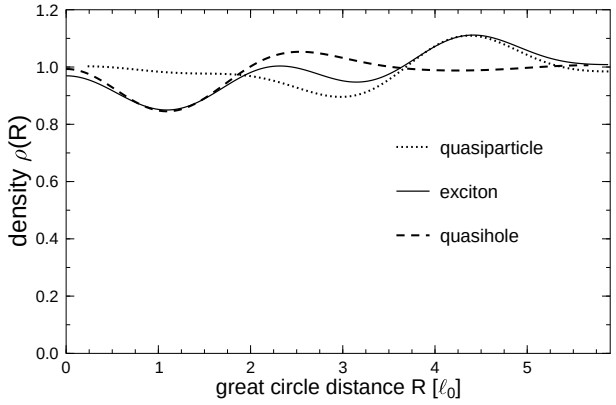

Figure 6: Density profiles of excitations at $\nu = 2/5$ as a function of great circle distance from the north pole: The $L = 8$ collective excitation (exciton) for the 14 particle system, the quasihole ($L = 7/2$) and the quasiparticle ($L = 4$) for the 13 particle system. The projection of angular momentum is maximal ($L_z = L$) in all cases. The origin for the quasiparticle has been shifted, so that the point at the south pole coincides with that for the exciton. In the thermodynamic limit, the exciton with these quantum numbers becomes a quasihole localized at the north pole and a quasiparticle localized at the south pole. It is clear that, even with 14 particles at $\nu = 2/5$, there is still significant overlap between the density variations associated the quasiparticle and the quasihole localized about opposite poles. This probably explains the large finite size effects seen (Figure 3) in the exciton energy as a function of N.

wavevector of a collective excitation is $k_{eff} = L/R$ where L is the total angular momentum of the system. This lowest-lying collective excitation should correspond to a well-separated quasiparticle-quasihole pair in the limit of large L. In the hierarchy picture, the separation of the particle and hole should be $2RL/N$, so the maximum separation possible occurs when $L = N_i$. Here N_i is the number of particles in the condensate of the highest (i'th) level of the hierarchy that occurs: $N_0 = N$, $N_1 = (N+2)/2$, $N_2 = (N+6)/3$ and $N_3 = (N+12)/4$ for $\nu = 1/3$, $2/5$, $3/7$ and $4/9$ respectively [3, 6, 10]. Extrapolations to the infinite system limit of the $L = N$ excitations should therefore give an estimate of the gap energies. The results for $\nu = 1/3$ and $2/5$ are also included in Fig 3. It is clear from the figure that an extrapolation based on the exciton energies would not be as smooth as that based on the charged excitations.

We believe that the exciton energies in the small systems accessible to direct diagonalization are not as reliable a basis for extracting estimates of the gaps as the sum of the quasihole and quasiparticle energies. The principal reason for this is that the quasihole and quasiparticle states are actually ground state configurations of N particles in total flux $2S_{\pm 1/p}$ and they are well-separated in energy from all excitations. On the other hand, although the neutral excitations are minimum energy states for the quantum numbers concerned, they are close to the continuum of excitations for these quantum numbers and this gives scope for large finite size effects, in addition to leading to poor convergence and numerical instability of vector iteration (Lanczos type) diagonalization methods. With the possible exception of the systems at $\nu = 1/3$, it is also clear that the system sizes accessible to direct diagonalization are not large enough to accommodate two excitations without significant overlap of the charge profiles of the quasiparticle and quasihole. In Figure 6, we show the density profile of the 14 particle exciton at $\nu = 2/5$, with the corresponding quasiparticle and quasihole density profiles for a 13 particle system overlaid for comparison. The quasiparticle and quasihole at the opposite poles are clearly visible, but the system is not large enough for the density profiles not to interfere.

V. INTERFACIAL WAVEFUNCTION AND MODIFIED INTERACTION

The finite width of the sub-band envelope wf in the direction perpendicular to the plane of the two-dimensional electron gas can be incorporated into an effective interaction between electrons in the plane. With the magnetic field perpendicular to the plane the single-particle orbitals can be written:

$$\Psi(x,y,z) = \zeta(z)\psi(x,y). \tag{13}$$

The in plane wf's $\psi(x,y)$ are eigenfunctions of the free electron Hamiltonian in a perpendicular magnetic field, while $\zeta(z)$ satisfies the Schrödinger equation for a particle in the confining potential of the quantum well or heterostructure [22]. The effective interaction between particles $V(|\vec{r}_1 - \vec{r}_2|)$ at positions $\vec{r}_1 = (x_1, y_1)$ and $\vec{r}_2$ in the two-dimensional electron gas is then given by

$$V(|\vec{r}_1 - \vec{r}_2|) = (e^2/\varepsilon) \int dz_1 \int dz_2 \frac{|\zeta(z_1)|^2 |\zeta(z_2)|^2}{\sqrt{(\vec{r}_1 - \vec{r}_2)^2 + (z_1 - z_2)^2}} \tag{14}$$

The study of finite-size systems is based on exact diagonalization or the study of variational trial wf's for particles in a given Landau level with the interparticle interaction

taken to be $V(|\vec{r}_1-\vec{r}_2|)$. For particles on a sphere, the interaction $V(|\vec{r}_1-\vec{r}_2|)$ projected onto a given Landau level is characterized by Haldane's pseudopotential parameters $\{V_m\}$ ($m=0,1,\ldots$). Once these are known the exact diagonalization proceeds exactly as in the zero-width case. (We note that as the pseudopotential parameters are computed from the effective interaction, which assumes a planar geometry, there is no attempt to account for any effects of the curvature of the sphere on the finite width effects.)

Within a local density functional scheme the wf $\zeta(z)$ satisfies the equation

$$\left(-\frac{\hbar^2}{2}\frac{d}{dz}\frac{1}{m^*(z)}\frac{d}{dz}+V_{eff}(z)\right)\zeta(z)=E\zeta(z) \qquad (15)$$

where $V_{\rm eff}$ includes the effect of the confinement potential (including the effect of the depletion layer), the Hartree self-interaction and exchange-correlation. For GaAs-GaAlAs quantum wells the jump in m^* and the dielectric constant, ε across the interface are small and to a good approximation both quantities can be taken to be independent of of z (see Table I in [36]) and the equation simplifies. In [22] this equation was solved numerically for various geometries and the results presented in the form of tables of pseudopotentials for quantum wells and heterostructures for various values of the electron density and device parameters. Here we show that the values of the pseudopotentials characterizing the Coulomb interaction in the finite-width geometries can be very accurately computed using a Gaussian and a new trial wf, the 'z×Gaussian' (zG), thereby allowing the effect on the pseudopotentials of a finite-width in the direction perpendicular to the 2D electron gas to be encoded in just one variational parameter, *ie* the width of the wf, parametrized by the standard deviation w of the probability density.

The self-consistent computation of $\zeta(z)$ and $V_{eff}(z)$ is standard and follows the procedure given in [22, 37]. The potential $V_{eff}(z)$ is written

$$V_{eff}(z)=V_W(z)+V_H(z)+V_{XC}(z) \qquad (16)$$

where $V_W(z)$ is the confining potential of the quantum well or heterostructure (including image charge effects and the effect of the depletion layer) and V_{XC} is the exchange-correlation potential

$$V_{XC}=\left[1+0.7734x\ln\left(1+x^{-1}\right)\right]\left(\frac{2}{\pi\beta r_s}\right)R \qquad (17)$$

where $\beta=(4/9\pi)^{1/3}$, $x=r_s/21$, $r_s=(4\pi a^* n(z)/3)^{-1/3}$, with $a^*$and R the effective Bohr radius and Rydberg in GaAs. The Hartree potential is given by

$$V_H(z)=\frac{2\pi e^2}{\varepsilon}\int dz\int dz'|z-z'|\left(|\zeta(z)|^2-\rho(z)\right)\left(|\zeta(z')|^2-\rho(z')\right) \qquad (18)$$

where $\rho(z)$ is the (neutralizing) charge density of the doping ions which are taken to be far way from the interface. In [37] V_H is referred to as the potential due to the induced charges or V_S. In the presence of N_A acceptors per unit volume in the semiconductor there will be n_{depl} ($=N_A z_D$) charges per unit area of the interface distributed evenly across the depletion layer of width z_D.

We obtain $\zeta(z)$ by solving (15) using trial forms for $\zeta(z)$ and compare the results with those obtained by numerical solution in [22]. The trial waveforms we have studied are the Fang-Howard (FH), which is zero for negative z and for positive z is given by

$$\zeta(z)\propto z\exp(-bz/2), \qquad (19)$$

the Gaussian

$$\zeta(z)\propto\exp(-(z-\alpha w)^2/4w^2), \qquad (20)$$

and the 'z×Gaussian' (zG) wf, which is again zero for negative z and for positive z is given by

$$\zeta(z)\propto z\exp(-z^2/9c^2). \qquad (21)$$

The width W of these wave functions can be characterized by the standard deviation of the corresponding probability density. It is given in terms of the parameters b,w,c as follows,

$$W_{FH}=\frac{\sqrt{3}}{b} \qquad (22)$$

for the Fang-Howard wf,

$$W_G=w \qquad (23)$$

for the Gaussian wf and

$$W_{zG}=\frac{3\sqrt{8+3\pi-16}}{2\sqrt{\pi}}c\approx 1.01016\times c \qquad (24)$$

for the zG wf.

We determine the parameters b, w, α and c variationally. We have found that, expanding the expression for V_{XC} in (17) in x and keeping only the constant and linear terms, reproduces the correct expectation value for the exchange-correlation energy to within 0.1% for all three trial wf's, while including the quadratic term affects only the fifth significant figure. The small x expansion works well because the dominant contribution to the exchange-correlation energy comes from the region in which the density is high (x small). Using this expansion allows us, for the three trial forms for $\zeta(z)$, to compute analytically all the integrals involved in computing $V_{eff}(z)$ and, hence, also the expectation value for the sub-band energy E. For the case of the Gaussian trial wf, the effective interaction (14) can be written in closed form in terms of the Bessel function K_0,

$$V_G(r)=\frac{1}{2\sqrt{\pi w^2}}e^{r^2/8w^2}K_0(r^2/8w^2). \qquad (25)$$

In Figure 7 we compare the estimates (see 15) of the sub-band energy for the three variational wf's: E(zG), E(Gauss)

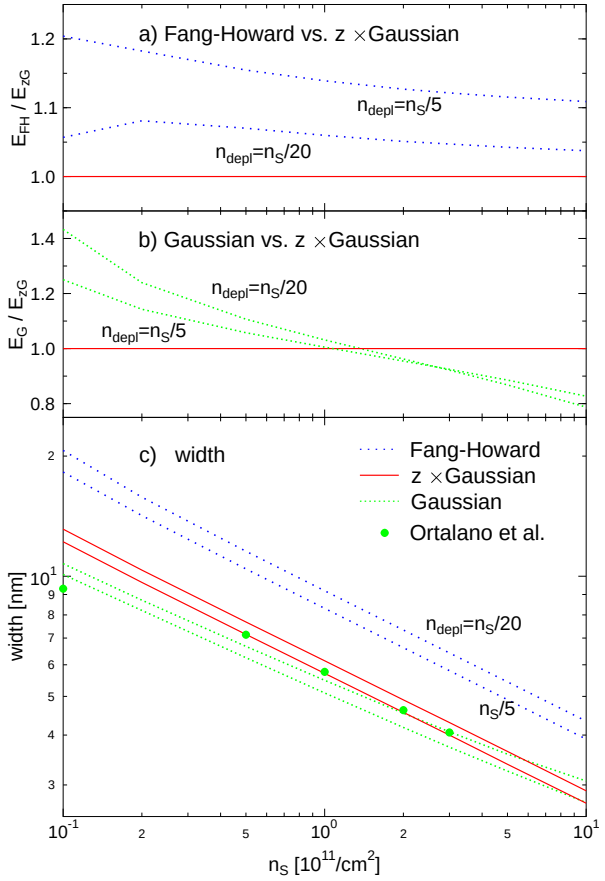

Figure 7: Comparison of the variational estimates for the sub-band energies (see 15) and of the standard deviation of the charge distribution (width) for the three variational wf's. The results for the width from direct numerical solution of the equation by Ortalano et al [22] are also included. The top panel shows the ratio of the variational estimates $E(\mathrm{FH})/E(\mathrm{zG})$ and the second panel shows $E(\mathrm{Gauss})/E(\mathrm{zG})$. The depletion layer density, n_{depl}, is quoted as a fraction of the electron density in the subband.

and $E(\mathrm{FH})$. For higher densities ($n_S \gtrsim 10^{11}/\mathrm{cm}^2$), $E(\mathrm{Gauss})$ gives the lowest variational estimate, while for lower densities $E(\mathrm{zG})$ gives the lowest estimate. For all densities in the range we have studied, we find that the Fang-Howard wf is worse as a variational wf than the zG and significantly worse at higher densities than the Gaussian. This is because the FH wf has too high a kinetic energy which it can only reduce by spreading the density wider. Although the variational estimate of the energy for the FH wf differs by a factor which only varies between 5% and 20%, the width of its distribution, as measured by the standard deviation, is significantly larger ($\sim 50\%$) than for the other two wf's.

Given that the integrals involved in using the Gaussian or zG wf's can be performed analytically and are more accurate as trial wf's, it is perhaps surprising that these wf's have not been more widely used in the study of heterostructures and quantum wells. Of the two, the Gaussian is easier to use, although it will be less well-adapted to MOS devices with large band gap discontinuities. For the heterostructures considered

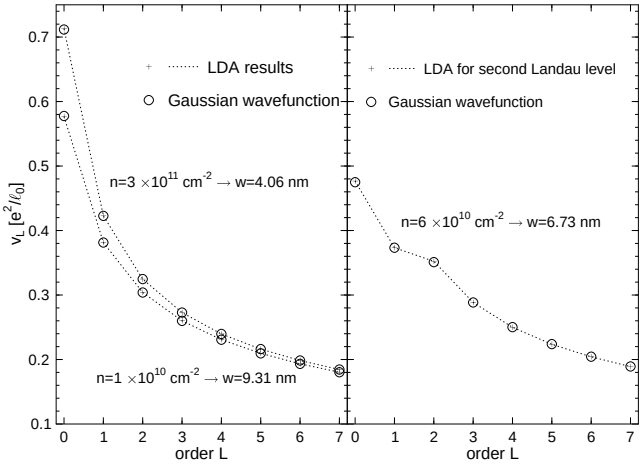

Figure 8: The Haldane pseudopotentials for the interaction $V_G(|\vec{r}_1 - \vec{r}_2|)$ (25) projected onto the lowest and second Landau levels as a function of angular momentum L for particles in heterostructures with densities n. The results of direct numerical solution of equation (15) taken from [22] are shown as crosses and results based on the Gaussian trial wf for $\zeta(z)$ as circles. The width parameter w of (20) for the trial wavefunction is chosen so that the Haldane pseudopotential V_1 matches that obtained by numerical integration. The differences between the results based on the Gaussian interface wave function and the numerically computed local density approximation is at the fraction of a percent level.

below we use a (conduction) band gap discontinuity of 200 mV - the value appropriate for a GaAs/$GaAs_{0.66}Al_{0.33}$ heterostructure. On the other hand, the 'zG', should become more favorable as a variational wf, when the band gap discontinuity is large and the effect of the boundary is well approximated by a hard wall.

Figure 8 shows the Haldane pseudopotentials for the interaction $V(|\vec{r}_1 - \vec{r}_2|)$ projected onto the lowest and second Landau levels for heterostructures with densities appropriate to samples studied experimentally. Here, we determine the width of the trial interfacial wf's by requiring that the Haldane pseudopotential V_1 from [22] is exactly reproduced. We note here, that results for the pseudopotentials in [22] were for a value of the magnetic length ℓ_0 which coincides with the Bohr radius $a_B^* \approx 10nm$ of electrons in GaAs. The results for the second Landau level were for the density $n_s = 6 \times 10^{10} cm^{-2}$ used in [22]. The study of the second Landau level in [22] was motivated by the results reported in [42] at filling fraction $\nu = 5/2$. However, the interfacial wave function is determined by the *total* number of electrons, which for the sample studied in [42] was $n_s \approx 3 \times 10^{11} cm^{-2}$, and not by the fraction occupying the second LL ($n_s^{(1)} = 6 \times 10^{10} cm^{-2}$) incorrectly used in [22]. For this reason, the conclusions regarding the $\nu = 5/2$ state of Reference [22] are incorrect.

It is clear that the use of the Gaussian trial wf yields results which are essentially indistinguishable from the results of the exact numerical solution for $\zeta(z)$. We find very similar results for the zG. In Figure 9 we show the difference between the pseudopotentials computed exactly by solving numerically for the interface wf $\zeta(z)$ (taken from [22]) and those obtained us-

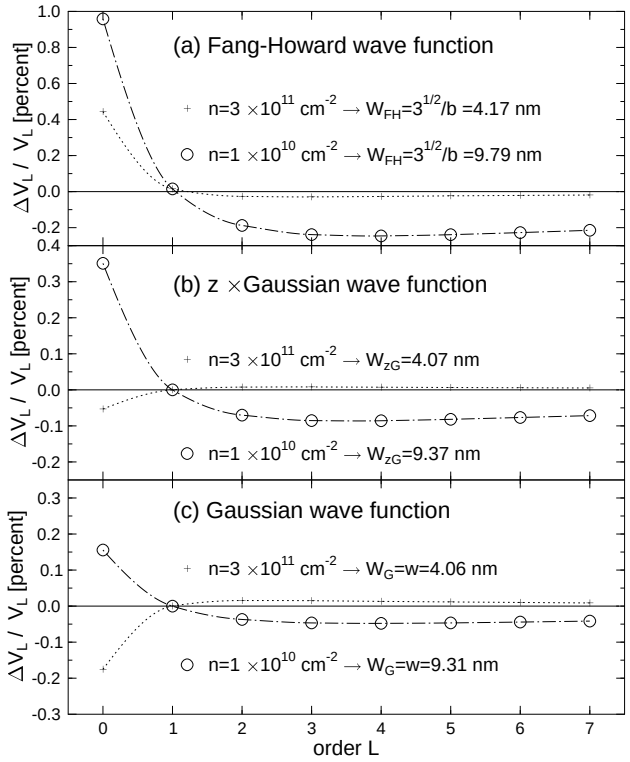

Figure 9: Errors in the Haldane pseudopotentials computed using the Fang-Howard, z×Gaussian (zG) and Gaussian interface trial wf's for two different densities. The comparison is with the values reported in [22]. The variational parameters are determined such that V_1 is correctly reproduced. The zG leads to errors for V_m, $m \neq 1$ which are roughly half as big as those with the Fang-Howard wf. The Gaussian wf is even better in reproducing the LDA results with a maximum error of less then 0.2 percent (for V_0). The width parameters for the three variational wavefunctions (given above each curve) are approximately equal for both densities for all three wavefunctions, implying that fixing the pseudopotential V_1 is effectively equivalent to fixing the standard deviation of the charge distribution.

ing the Gaussian and FH wf's. The errors obtained using the FH wf are at the 1% level while those obtained for the Gaussian are at the 0.1% level. Those obtained using the Gaussian trial wf are smaller than other uncertainties in the model such as those related to the value chosen for the depletion density, n_{depl}. Finite-width effects on the Haldane pseudopotentials are clearly accurately captured by the Gaussian (and zG) trial wf's. Given the fact that the pseudopotentials V_m only depend on the width parameter (w for the Gaussian wf, b for the Fang-Howard wf and c for the zG), it is clear that the use of these trial wf's massively simplifies the study of finite-width effects when compared to the numerical integration of (15) and tabulation of pseudopotentials used in [22]. For the case of the Gaussian, we also have an analytic expression for the effective interaction $V(|\vec{r}_1 - \vec{r}_2|)$, cf equation (25).

The tables I-IV of reference [22] can be summarized by listing the effective width of the Gaussian interface wf for which the Haldane pseudopotential of order $m = 1$ is exactly reproduced. In Table I we list the width parameters for all tabulated cases.

I parabolic QW		II Heterointerface		III square QW		IV Heterointerface	
n_s	$w[nm]$	n_s	$w[nm]$	n_s	$w[nm]$	n_s	$w[nm]$
0.49	19.3813	0.10	9.30690	0.10	3.21628	0.60	6.72784
0.60	24.1478	0.50	7.13556	0.50	3.21854		
0.73	28.9638	1.00	5.76001	1.00	3.22610		
0.85	33.1890	2.00	4.61801	5.00	3.31037		
		3.00	4.06015				

Table I: Width parameters for all tabulated results of Reference [22]. The electron density n_s is measured in units of $10^{11}/cm^2$ while the width w of the interfacial wf is given in *nm*.

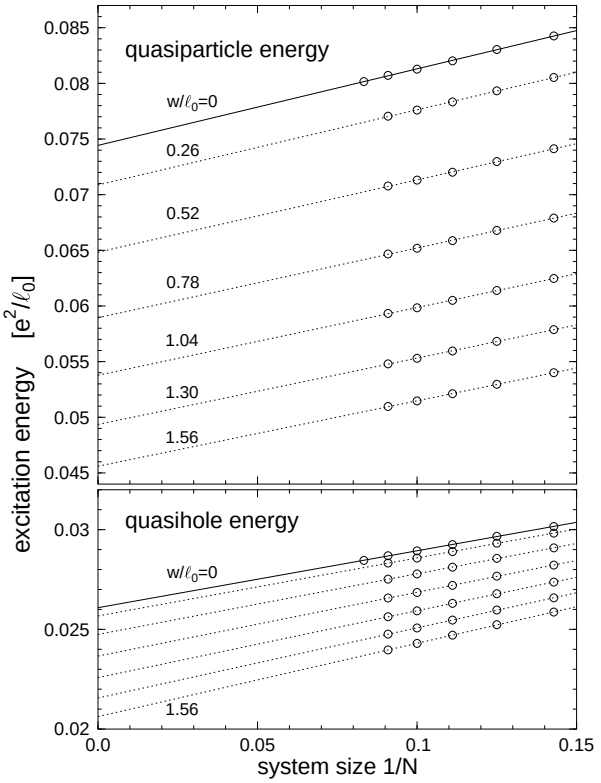

Figure 10: The quasihole energy $\widetilde{e}^{+}_{1/3}(N)$ and quasiparticle energy $\widetilde{e}^{-}_{1/3}(N)$ and the best linear fits to these points computed as a function of the width w of the density distribution computed using Gaussian trial wf's. The sum of the two linear functions can be taken as a measure of the gap energies $\widetilde{e}^{g}_{1/3}(N)$.

VI. FINITE WIDTH EFFECTS ON ENERGY GAPS

A. Filling fractions $\nu = \frac{p}{2p+1}$

With these modified potentials we have repeated the calculations described in section 2. Using the Gaussian wf parametrized by its width w we compute the Haldane pseudopotentials as a function of w. By exact diagonalization just as in the pure Coulomb case of Section 3, we compute width dependent excitation energies for all possible system sizes and

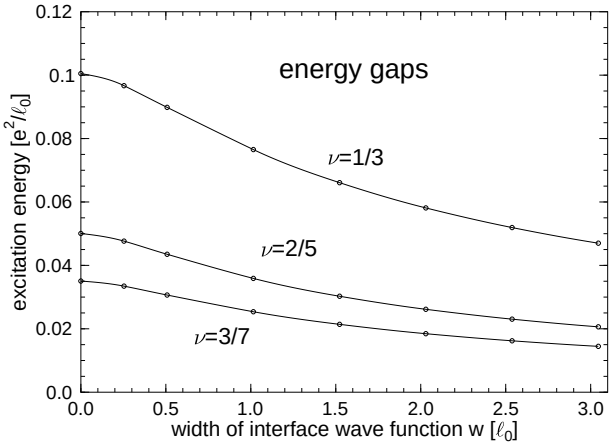

Figure 11: Estimates of the energy gaps in the thermodynamic limit as a function of the width of the subband wf (taken as the standard deviation of the charge distribution). The solid lines show the fits to the interpolation formula (cf. Equation (26) and Table II).

ν	$E_G^{(0)}$ [$\frac{e^2}{\varepsilon\ell_0}$]	ϕ [degrees]	a	b
1/3	0.1012	34.18	0.1468	1.542
2/5	0.0500	36.07	0.1935	1.866
3/7	0.0350	34.98	0.2078	1.851

Table II: Interpolation function for the gap energy as a function of width (26): parameters for filling fractions $\nu = 1/3,\ 2/5,\ 3/7$.

perform for each value of the width parameter w an extrapolation to the thermodynamic limit $N \to \infty$. As an example we show in Figure 10 the size and width dependent quasiparticle $\widetilde{e}^{-}_{1/3}(N)$ and quasihole energies $\widetilde{e}^{+}_{1/3}(N)$ at $\nu = 1/3$. For each width w we use linear extrapolation in $1/N$ to estimate the gap energy in the thermodynamic limit as a function of width. The size dependence at finite width is qualitatively the same as at $w = 0$. This same procedure was also employed for the calculation of width dependent quasiparticle and quasihole energies at $\nu = 1/3$ and $\nu = 2/5$, and the corresponding energy gaps in the thermodynamic limit. The result of these calculation are shown in Figure 11. The full lines in Figure 11 correspond to interpolation functions of the form

$$E_G(x) = E_G^{(0)} \times \left(\frac{\cos^2\phi}{\sqrt{1+ax^2}} + \frac{\sin^2\phi}{1+bx^2}\right), \qquad (26)$$

where $x = w/\ell_0$. The functional form (26) is suggested by the following observations: The Haldane pseudopotentials V_m for $m > 0$ behave for $w \to 0$ as $V_m \approx V_m^{(0)} + O(w^2)$ while for very large w they behave as $V_m \approx (\log(w)/\sqrt{\pi} + \alpha_m)/w$. Indeed, as will be seen below, the energy gaps decrease as $1/w$ for very large values of the width w, implying that the logarithmic term cancels out in this limit. The values of the fitting parameters $E_G^{(0)}, \phi, a$ and b are listed in Table II for the filling fractions $\nu = \frac{1}{3}, \frac{2}{5}, \frac{3}{7}$.

The results presented in Figure 11 are similar to those reported in [25]. The results of [25] were based on Monte Carlo simulations (MC) of CF trial wavefunctions, which as mentioned in section IV, give larger gaps than our results for the bare Coulomb interaction even at $\nu = 1/3$. This discrepancy exists throughout the range of w/ℓ_0 in the figure with our estimates being between $\sim$5% smaller (for $\nu = 1/3$) and $\sim$ 25% smaller (for $\nu = 3/7$ and $4/9$). (It is not surprising that the difference does not depend strongly on w/ℓ_0: While the energies are affected by the width w through the variation of the effective interaction, the wavefunctions are not expected to change significantly [6].) The gaps as a function of width have also been estimated [43] using a field theoretic approach [43], which constructs explicit CF wavefunctions out of Chern-Simons gauge-transformed fermions. Energies of ground and excited states can be computed within this theory at the Hartree-Fock level. The theory needs to cut off the interaction at large wavevectors and should therefore be reliable for large widths where the inverse width provides a natural large wavevector cut-off. For widths $w/\ell_0 \gtrsim 2$, the results are consistent with those of the MC simulations using composite fermion trial wf's [25]. For $0.5 < w/\ell_0 < 2$, the results are still comparable to those of the MC simulations, although they imply gaps which are rapidly increasing as $w/\ell_0 \to 0$, in contrast to the results in Figure 11.

Evidence, also based on CF trial wavefunctions, was presented in [23] which suggested a phase transition as a function of increasing width from incompressible states to compressible states at filling fractions $\nu = p/(2p+1)$. We have tested this theoretical prediction by computing the width dependent energy of the lowest energy excitation, which corresponds to the roton minimum. We have not analyzed the extrapolation to the infinite-system size limit for the roton minimum and present, instead, the variation with width of the roton minimum energy for a system with fixed particle number. We show the results for $\nu = 1/3$, $2/5$ and $3/7$ in Figure 12. We find that even for very large and unphysical widths up to hundreds of nanometers (corresponding to up to $50\,\ell_0$), there is no evidence of the gap vanishing at any of these filling fractions. Instead we find that for such large width parameters the roton minimum scales simply as $1/w$.

B. $\nu = \frac{5}{2}$ state

Here, we present the results of calculations of the finite width effect on the energy gap of the mysterious $\nu = 5/2$ state. If the effects of Landau level mixing are neglected, it is sufficient to solve for the ground state of the electrons occupying the second - half-filled - Landau level and take the filled lowest Landau levels of spin-up and spin-down electrons as inert, i.e. unpolarizable. This problem is characterized by a filling factor $\nu^{(1)}$ of the first excited Landau level of $\nu^{(1)} = 1/2$. It is customary to represent the system of electrons filling half the second Landau level by lowest Landau level wave functions but to take into account the interaction of electrons in the second Landau level by using the appropriate Haldane pseudopotentials of the second Landau level. Again, as for the computation of energy gaps at $\nu = p/(2p+1)$, there are essentially two ways to compute the energy. Either one may

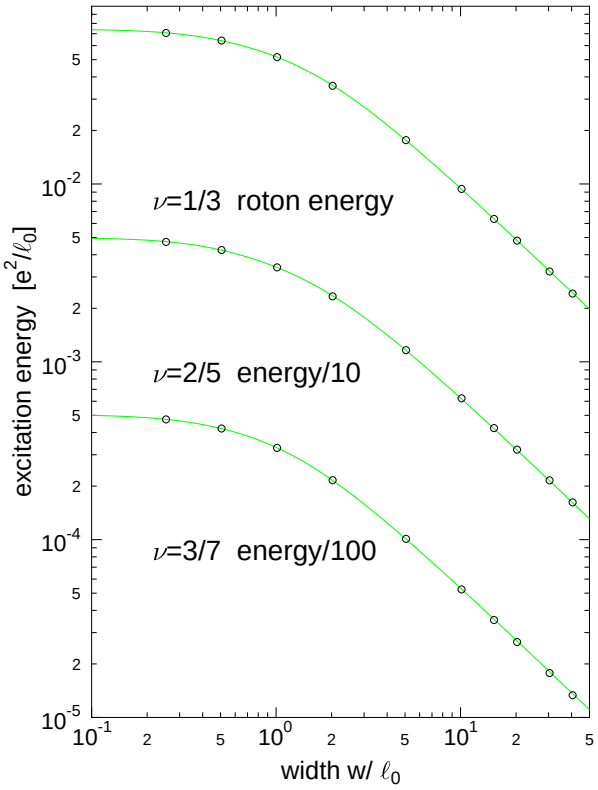

Figure 12: The energy of the roton minimum as a function of width for systems with 11 particles at $\nu = 1/3$, 14 particles at $2/5$ and 15 particles at $3/7$. For clarity, the energies of the roton are scaled by a factor 1/10 at $\nu = 2/5$ and 1/100 at $\nu = 3/7$. If there were to be phase transition to a compressible state the gap would have to vanish at some finite width. Instead we find clear evidence that, for large widths, the energy of the roton minimum (the lowest-lying excitation at fixed total flux) tends to zero as $1/w$ with no suggestion of a phase transition.

calculate neutral excitation (exciton) energies corresponding to a widely separated quasiparticle and quasihole pair, or one may calculate the energy of ground states containing a (fractionally) charged excitation. In the case of the $\nu = 5/2$ state, or equivalently at $\nu^{(1)} = 1/2$, there is the problem that elementary charged excitations are predicted to occur only in pairs.

The polarized ground state at $\nu^{(1)} = 1/2$ occurs on the sphere when the number of flux units is

$$2S_0 = 2N - 3, \tag{27}$$

and is thought to be described by a paired state, which may be of the Moore-Read pfaffian type [31, 32, 45]. However, great care is needed when analyzing excitation energies in these states on the sphere to avoid mistaking systems at conventional filling fractions $\nu_p = p/(2p+1)$ or $1-\nu_p$ for systems at filling $\nu^{(1)} = 1/2$. As we have discussed previously [10], systems on the surface of a sphere exhibit degeneracies where, for a certain size N, states with different filling factor coincide. This turns out to be a particularly severe problem in the sequence (27). Indeed, of the possible systems with

N	$2S_0$ (GS)	ν_a	$2S_0+1$	ν_a	$2S_0-1$	ν_a
6	9	2/3	10		8	
8	13		14		12	2/3
10	17		18		16	
12	21	3/5	22		20	
14	25		26		24	
16	29		30	4/5	28	
18	33		34		32	

Table III: Total flux in the ground ($2S_0$) and excited ($2S_0 \pm 1$) states for systems at $\nu^{(1)} = 1/2$ as a function of number of particles, N. Where these states are aliased to conventional quantum Hall state ground states, we also show the corresponding filling fractions, ν_a. We note that the only sizes for which no aliases occur, are $N = 10, 14$ and 18. Unaliased ground states occur in addition at $N = 8$ and 16.

up to 18 electrons, only five are not aliased with conventional fractional states, namely those with $N = 8, 10, 14, 16$ and 18 particles. Of these, the ones at $N = 8$ and 16 have the problem that charged excitations of these states are aliased with ground states of conventional FQH states. Using these aliased states for a calculation of the energy gap at $\nu^{(1)} = 1/2$ would be misleading and would give rise to systematic errors. In Table III, we list the relevant states and their aliases. We first show the energy of neutral excitations (exciton) with maximal angular momentum L_{max}, corresponding to the largest possible separation of the quasiparticle and quasihole on the sphere. The angular momentum of this exciton is given by $L_{max} = N/2$ if $N/2$ is even, otherwise $L_{max} = N/2 - 1$. In Figure 13 the exciton energy for zero width, corrected for the Coulomb attraction between quasiparticle and quasihole ($A_{1/4}(1/2)$, equation (6), is plotted as a function of system size $1/N$ together with a linear fit in $1/N$ to the data at $N = 8, 10, 14, 16$ and 18, cf. Table III. Like at $\nu = 2/5$, the exciton energy shows very large, and fluctuating finite size effects. Extrapolation to the bulk limit using a linear fit in $1/N$ yields the result

$$\Delta_{5/2}^{exc} \approx 0.028 \frac{e^2}{\varepsilon \ell_0}. \tag{28}$$

Alternatively, the energy gap can also be computed by calculating individually the energy of quasiparticle and quasihole excitations. The two quasiparticle state occurs at $2S_0 - 1$ while the two quasihole state occurs for $2S_0 + 1$. Since in both cases the two excitations have the same charge ($q = e/4$ for the quasiparticle and $q = -e/4$ for the quasihole), one expects that the lowest energy state occurs when the two charges are maximally far apart, which demands maximum relative angular momentum, and consequently minimum total angular momentum on the sphere. Although one might have expected that this would imply $L = 0$ for the ground state, as a result of symmetry, the angular momentum of the lowest energy states is $L = N/2 \, mod \, 2$, i.e. $L = 1$ for $N = 10, 14, 18$. The energy of these two-quasiparticle or two-quasihole states contains, in addition to the term $A_{2q}(\nu^{(1)})$ (equation 6), the Coulomb interaction, ΔA_q, of two quasiparticles separated by twice the radius R (the maximal separation on the sphere):

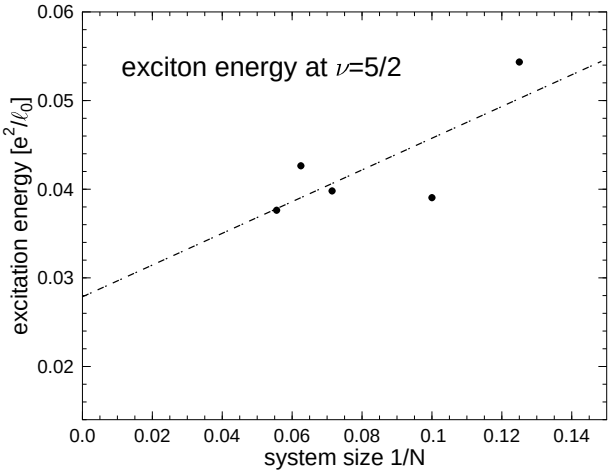

Figure 13: The exciton energy at $\nu = 5/2$ for zero width, corrected for the Coulomb attraction between quasiparticle and quasihole ($A_{1/4}(1/2)$, equation (6), is plotted as a function of system size $1/N$.

$$\Delta A_q = q^2\sqrt{\frac{\nu^{(1)}}{2N}}. \tag{29}$$

Combining the two contributions $A_{2q}(\nu^{(1)})$ and ΔA_q gives for the finite size correction term $C_q(N)$

$$C_q(N) = -3q^2\sqrt{\frac{\nu^{(1)}}{2N}} = -\frac{3}{32}\sqrt{\frac{1}{N}}. \tag{30}$$

The gap calculation then proceeds by taking account explicitly of the finite size correction $C_q(N)$ (equation 30), as described for the cases at $\nu = p/(2p+1)$ in the previous section.

In Figure 14(a), we show our results for the gap at $\nu = 5/2$. In the top figure, half the sum of quasiparticle and quasihole excitation energies are plotted as a function of system size $1/N$ for different values of the width w. For zero width, results for $N = 10, 14$ and 18 are plotted, the sizes at which no aliasing effects occur. They lie almost exactly on a straight line in $1/N$. Extrapolation to the bulk limit yields

$$\Delta_{5/2} \approx 0.025\frac{e^2}{\varepsilon\ell_0}, \tag{31}$$

slightly lower, but consistent with the result (28) based on the exciton energies. Based on our previous experience with gap calculations at $\nu = 1/3$ and 2/5, we believe that also at $\nu = 5/2$ the extrapolation based on individual quasiparticle and quasihole energies is more reliable. However, the exciton energy calculation certainly supports our conclusion that the quasiparticle and quasihole states at $\nu = 5/2$ contain two charged defects. Otherwise, there would be a factor of two difference between our extrapolated values $\Delta^{exc}_{5/2}$ (equation 28) and $\Delta_{5/2}$

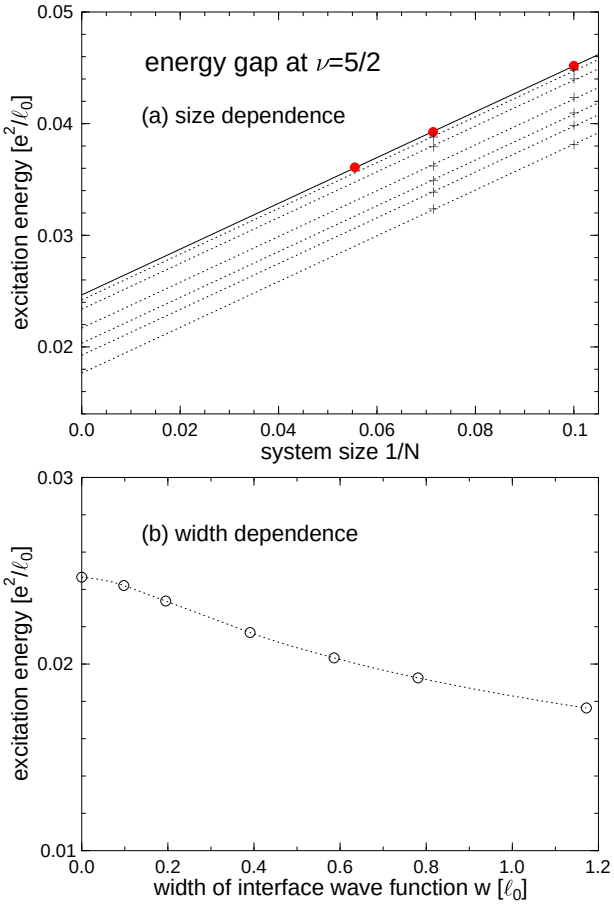

Figure 14: Energy gap at $\nu = 5/2$. The upper panel illustrates the size dependence of the energy gap for different values of the width parameter $0 \le w/\ell_0 \le 1.17$. The width parameters are $w/\ell_0 =$ 0, 0.098, 0.195, 0.391, 0.586, 0.781, 1.17,with the topmost line referring to the case $w = 0$, and the rest in sequence down to the lowermost line with $w/\ell_0 = 1.17$. The extrapolations to the $N \to \infty$ limit assume that the slopes for the cases with $w \neq 0$ are the same as for the $w = 0$ case. In the lower panel the gap values, extrapolated to the $N \to \infty$, are plotted as a function of w/ℓ_0.

(equation 31). Finally, in Figure 14(b), the gap in the thermodynamic limit is plotted as a function of width w/ℓ_0. These results indicate that the width effects reduce the gap at $\nu = 5/2$ slightly.

Very recently, Eisenstein et al [46] have investigated the $\nu = 5/2$ and 7/2 states in a sample of ultra-high mobility ($\mu \approx 3.1 \times 10^7 \mathrm{cm}^2/\mathrm{Vs}$). They determined an activation gap $\Delta^m_{5/2} \approx 0.31$K at $\nu = 5/2$ and $\Delta^m_{7/2} \approx 0.07$K at $\nu = 7/2$. Their sample had an electron density $n_s = 3 \times 10^{11}/\mathrm{cm}^2$, which leads to a width $w \approx 4$nm. At $\nu = 5/2$, the field $B = 4.96$T corresponds to a value $w/\ell_0 \approx 0.35$, while at $\nu = 7/2$ we get $w/\ell_0 \approx 0.30$. According to the results shown in Figure 14, The calculated gap values (see Figure 14) for $w/\ell_0 \approx 0.35$ and 0.30 are around 0.0220 and $0.0225e^2/\varepsilon\ell_0$ respectively. These lead to theoretical values for the gap of $\Delta^m_{5/2} \approx 2.5$K and $\Delta^m_{7/2} \approx 2.1$K. A disorder broadening of the order of 2K would explain the measured gaps of 0.31K and 0.07K. It is

	Sample A ($\Gamma = 1.28 \pm .13$K)				Sample B ($\Gamma = 2.1 \pm .17$ K)			
ν	B[T]	$\Delta_\nu^m + \Gamma$ [K]	Δ_ν^c [K]	$\frac{\Delta_\nu^m+\Gamma}{\Delta_\nu^c}$	B[T]	$\Delta_\nu^m + \Gamma$[K]	Δ_ν^c[K]	$\frac{\Delta_\nu^m+\Gamma}{\Delta_\nu^c}$
1/3	13.9	9.03	15.2	0.59	28.5	13.2	18.9	0.70
2/5	11.6	4.48	6.9	0.65	23.8	6.5	8.6	0.75
3/7	10.8	3.23	4.8	0.67	23.2	4.5	5.7	0.79
4/9	10.4	2.23	3.6	0.61	21.4	3.3	4.9	0.68

Table IV: Comparison of the measured gaps, Δ_ν^m, in samples A (nominal density 1.12×10^{11} cm^{-2}) and B (nominal density 2.3×10^{11}cm^{-2}) reported in [12] with the gaps computed for a Coulomb interaction but taking account of the finite-width effects, Δ_ν^C. We have added a constant field-independent shift, Γ, for each sample which we estimate by comparing the functional dependence of the gap energies as a function of filling fraction, ν, predicted by CF theory with that found in experiment. The range quoted for Γ gives the maximum and minimum found when the constant C' in (10) varies between 4.11 (our estimate of C' for the pure Coulomb interaction) and 9.

ν	B[T]	Δ_ν^m [K]	Δ_ν^c [K]	Δ_ν^w [K]
1/3	21.0	10.5	16.6	13.5$\pm$.5
2/3	10.8	6.5	13.1	10.7$\pm$.5
5/3	4.5	1.0	9.3	7.9$\pm$.3

Table V: The activation energies as deduced from the temperature dependence of the longitudinal resistivity at filling fractions $\nu = 1/3, 2/3, 5/3$, Δ_ν^m, reported in [11] are compared to our values for the gaps, Δ_ν^c. For reference, we also show the calculated values of Willett et al. [11] in the last column. These authors fixed the depletion density n_{depl} and hence the width parameter w by requiring that the solution of (15) correctly reproduced the experimentally measured sub-band splitting. They estimated the finite width corrections on the basis of the model interaction (32) to give Δ_ν^w .

important to note that previous experimental values of the excitation gap at $\nu = 5/2$ have been much smaller [47, 48]. For samples with density $n_s = 2.3 \times 10^{11}$/cm^2 the gap at $\nu = 5/2$ was 0.11K [48]. In this case, the width is $w \approx 4.5$nm, and at the field $B = 3.65$T, we obtain $w/\ell_0 \approx 0.34$, and a theoretical gap value of 2.1K. The factor of ~ 3 difference between the recently reported activation gap [46] and the earlier estimate [48] in samples with similar densities suggests that the activation gap is affected strongly by sample quality, and is likely to be dominated by the effects of disorder. By comparing the gap at 5/2 to those at 7/3 and 8/3, and also at $\nu = p/(2p+1)$, Pan et al. also concluded that a disorder broadening of the order 2K was to be expected.

VII. EXPERIMENTAL GAPS

Estimates of the gaps for fractional quantum Hall systems have been reported for GaAs heterojunctions [11, 12] and more recently for metal-insulator-structures (MIS) using organic (pentacene and tetracene) semiconductor layers [49]. The recent measurements on organic MIS structures are particularly interesting given the different separation of energy scales to that found in GaAs. The dielectric constant in tetracene is in the range $\varepsilon \approx 3$ to 4 (compared to $\varepsilon \approx 12.7$ in GaAs), the band mass is $\sim 1.3 m_e$ (0.07 in GaAs) and the g-factor is close to 2 (0.44 in GaAs). The larger band mass and the smaller dielectric constant mean that, for samples with the same density, the ratio of interaction energies to the Landau-level splitting is much larger in the tetracene structures than in GaAs and hence that Landau level mixing effects are expected to be larger. The larger g-factor gives a larger Zeeman energy, and hence makes spin-reversed excitations less likely than in GaAs heterostructures.

We have estimated the gaps at $\nu = 1/3$, $2/5$ and $3/7$ for the two samples A and B of [12]. We take the quoted density of the samples and assume a depletion density $n_{depl} = n_S/5$ (this is typical of these samples [11], although the results are not sensitive to the exact value of n_{depl}). ¿From the results in Fig 7 we estimate the standard deviation of the density distribution and this leads directly to an estimate of the gaps (see Fig 11). We compare our results with those of the two samples A and B of [12] in Table IV. The effects of impurity scattering have been taken into account empirically by assuming that the levels are broadened by a field-independent broadening Γ. This assumption has not been theoretically justified, However, for the purpose of comparison we have reanalyzed the results of [12] under this assumption by fitting them to the functional form predicted by CF theory, i.e. including the logarithmic corrections (see 10) to extract the broadening Γ. We find that the gaps measured are consistently between 60 and 70% of what we predict after taking account of finite thickness effects. This is consistent with the results of [24, 25], correcting the error of Reference [23].

The results reported in [11] relate to filling fractions $p/3$, where $p = 1$, 2, 4 and 5 and were interpreted on the assumption that the ground states and gaps were all maximally spin-polarized states within the lowest Landau level for a sample with density $n_s = 1.65 \times 10^{11}$ cm^{-2} and mobility 5×10^6 cm^2/V sec (to be compared with 6.8 and 12×10^6 cm^2/V sec in samples A and B in [12]). The authors of [11] solved (15) numerically for the sub-band wf, $\zeta(z)$, choosing the depletion density n_{depl} to reproduce the experimentally observed sub-band splitting. As as a result we have a more precise estimate of width of the wf in the lowest sub-band than we have been able to make for the samples of [12]. We have converted their estimate of the width to a standard deviation w and estimated the gaps at the relevant filling fractions. The results are presented in Table V. We note that the measured values Δ^m of the gap at $\nu = 1/3$ and 2/3 are both larger than our theoretical values by about the same amount $\Gamma \approx 6$K. This might serve as an estimate of the broadening. The authors of [11] also estimated the gap reduction on account of finite thickness effects based on the exact diagonalizations of six particle systems reported in (32) and we include these estimates Δ_ν^w in the Table. The reduction of the gaps found in the earlier finite-size studies was significantly larger than what we obtain (Section 3). It may have resulted from estimating the gap reduction using systems which were too small, or inaccurate extrapolation to the thermodynamic limit.

It is clear from both Tables IV and V that the discrepancy between measured gaps and computed gaps is significant. This discrepancy may be due to Landau level mixing, spin-reversed excitations and to impurity effects not accounted for by the use of the field-independent broadening Γ used in Table IV. Estimates in [21] based on diagonalizations of up to only 5 particles in a torus geometry suggested reductions of the gap (identified with the zone boundary exciton) as a result of Landau level mixing of between 12% and 17% were possible at $\nu = 1/3$ in a magnetic field at 10T for a pure Coulomb interaction. These should scale as $(e^2/\varepsilon\ell_0)/\hbar\omega_c \sim 1/\sqrt{B}$. On this basis the reduction at a field of 28.5T for sample B at $\nu = 1/3$ would be at most 10%. However, as the matrix elements between Landau levels of the effective interaction $V(|\vec{r}_1 - \vec{r}_2|)$, which diverges only logarithmically as $r \to 0$, will be significantly smaller than those of the bare Coulomb interaction, the reduction of the gap due to Landau level mixing in these samples should, in fact, be significantly smaller than this figure of 10% and is probably negligible. Clearly, a new study along the lines of [50] (which actually looked at the harder problem of Landau-level mixing at $\nu = 5/2$ for systems with a partially filled second Landau level), taking account of the finite-width of the subband wf, would make for significantly more accurate estimates of Landau level mixing effects.

We should also consider the role of excitations involving spin reversals. The gap at $\nu = 1/3$, corresponding to the creation of a quasihole with no spin-reversal and a quasiparticle with one spin-reversal, was estimated in [9, 51] using extensive Monte Carlo simulations of trial wf's. Gap estimates for various combinations of quasihole and quasiparticles combined with spin-reversals based on exact diagonalizations of small systems (up to six particles) were reported in [29]. For the case of the pure Coulomb interaction and ignoring the Zeeman energy the gap to create spin-reversed excitations was around 60% smaller than the spin-polarized gaps for systems at $\nu = 1/3$. When the Zeeman energy (in GaAs) is taken into account this suggests that, for a pure Coulomb interaction, the spin-reversed excitation would have a lower energy for systems at $\nu = 1/3$ if the magnetic field were smaller than ~ 7T. This is above the fields at which the $4/3$ and $5/3$ states were observed in [11] (see Table V), and may account for the larger discrepancy seen at these filling fractions than at $\nu = 1/3$ or $2/3$.

The estimate of 7T, as the field below which the spin-reversed excitation drops below the spin polarized excitation, is well below the fields in Table IV making it unlikely that spin-reversed excitations are involved at these filling fractions. Although the explicit estimate of the spin-reversed excitation was made for a system at $\nu = 1/3$ it is unlikely that the discrepancy at other filling fractions will be larger. This is because the difference between the spin-polarized and spin-reversed quasiparticle energies should be largest at $\nu = 1/3$, where it is possible to construct a spin-reversed quasiparticle state which is a zero-energy eigenstate of the hard-core potential (with only the pseudopotentials V_0 and V_1 non-zero). For the case of the Coulomb interaction, its energy is controlled by the size of the pseudopotential V_2, while the energy of the spin-polarized quasiparticle is determined by the larger V_1. However, as V_2 is reduced less by finite width effects than V_1 (see Figure 9), the spin-polarized quasiparticle will be stabilized with respect to the spin-reversed excitation by finite-width effects [9].

The results for the activation gaps at $\nu = 1/3$ and $2/5$ in layers of tetracene reported in [49] can also be compared with our numerical results. By simultaneously varying the gate voltage and magnetic field the gaps could be tracked as a function of the ratio w/ℓ_0 for a range of fields $3 < B[T] < 9$. One intriguing feature of these organic layers is that the ratio of the Coulomb interaction to Landau level spacing, $(e^2/\varepsilon\ell_0)/\hbar\omega_c$, is approximately 30-40 times larger than in the GaAs samples for systems at the same magnetic fields.

We have computed the width, w, of the subband wavefunctions in the tetracene samples of [49] excluding the effects of image charges using the zG trial wavefunction and found that w varies between $17\AA$ at a density $n_s = 0.1 \times 10^{11}$ cm^{-2} and $7\AA$ for $n_s = 5 \times 10^{11}$cm^{-2}. The effects of the image potential will be to reduce the width still further. At all the densities, at which the gaps were measured, $w/\ell_0 < 0.1$ and so the effects of the finite width of the wavefunction on the gaps in these samples are small (see Fig 11) and significantly smaller than were reported in Reference [49, 53]. However, our calculations summarized in Fig 11 are a more accurate reflection of finite width effects than the old formula of [20] used in [49]. We also note that the widths we obtain are about half the order of magnitude ($w \sim 35\AA$) quoted in [49].

In order to compare the results of our calculations with the results of the experiments on the tetracene MIS structures, we need to take account of the large difference between the dielectric constant of the alumina insulating layer ($\varepsilon \sim 9.8$) and the value for tetracene ($\varepsilon \sim 3.5$). Nearly all the charge density is within $3w$ of the interface. This is significantly less than the average interparticle spacing or ion disk radius ($a = \sqrt{2/\nu}\ell_0$), which for these samples varies from $150\AA$ to $360\AA$ depending on density. We have used the simplest approximation which treats the 2D electron gas as if it were trapped at the interface of the alumina and the semiconductor. The effective dielectric constant is then just the average for the two materials. (Corrections to this, taking account of the actual displacement of the charge away from the interface, would involve image charge effects and give rise to a change in the functional form of the effective interaction between particles [52].) In Figure 15, we compare the results we obtain with the measured values reported in [49]. We show calculated gaps as a function of magnetic field ignoring the finite width of the charge distribution.

The difference between the computed and measured values of the gaps in Figure 15 at $\nu = 1/3$ and $2/5$ are remarkably small. Although there is some uncertainty associated with the computed gaps arising from the simple treatment of the large difference in dielectric constant of tetracene and alumina, there is surprisingly little evidence of large Landau level mixing (LLM) or disorder-related effects at these filling fractions. The ratio of the Coulomb energy scale $e^2/\varepsilon\ell_0$ to the cyclotron energy in tetracene is $\sim 93/\sqrt{B}$ or ~ 42 at $B = 5$T and LLM should be significant and might even be expected to be dramatic. When the ratio of these two energy scales is this

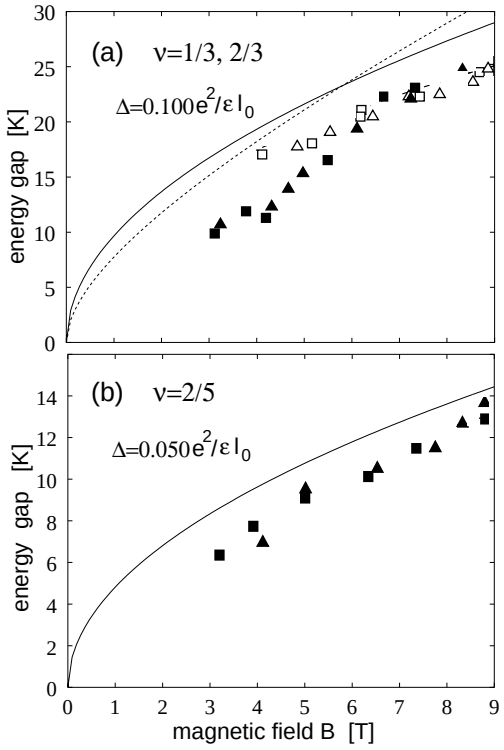

Figure 15: Gap energies at $\nu = 1/3$ (upper panel, unfilled symbols) and $2/3$ (upper panel, filled symbols) and $2/5$ (lower panel) in tetracene samples from [49] compared with numerical estimates. Triangles and squares denote experimental results for different samples. The solid line in each panel shows the gap given by the quoted formula which is valid in the zero thickness limit (as discussed in the text the effects of the non-zero width are negligible in these samples). The effective dielectric constant is taken as the average $\varepsilon = 6.65$ of reported values for tetracene $\varepsilon = 3.5$ and the value $\varepsilon = 9.8$ for the alumina insulating layer. The dashed line in the upper panel is an estimate of the energy gap for spin reversed excitations (see text).

large a perturbative treatment of LLM effects may not even be possible. (We have assumed the same effective dielectric constant as used in Fig 15). Even though the mobilities are not as high in the tetracene MIS structures as in the GaAs-GaAlAs heterostructures [11, 12], the agreement between calculated and measured gaps suggest that there are not any strong effects of disorder scattering either.

For the systems at $\nu = 2/3$ (filled symbols in upper panel of Fig 15), it was suggested in [49] that the change in slope at around 6.5T was related to a transition from a polarized state at high fields to a state which was not fully polarized at lower fields. This seems unlikely. At a transition with a discontinuity in polarization (first order transition), there would normally be a discontinuity in the gap rather than a discontinuity in its gradient with magnetic field, see for example [54]. There has been one report of a transition from a polarized to partially polarized state at $\nu = 2/3$ in GaAs heterostructures without any discontinuity of the gap [55]. However the corresponding transition would be expected to occur in the tetracene samples at around 1.7T well below the range of fields of Fig 15. Even if there were no (or only a small) discontinuity in the gap, the change in slope would normally be in the opposite sense to the one reported (see Figure 15). The lowest-lying excitations from a partially polarized (or unpolarized) state would be expected to involve spin reversals which increased the total aligned spin (rather than reduced it) and thereby gained a reduction in Zeeman energy. On the other hand, excitations from the fully polarized state, either decrease the total spin or leave it constant. As a result there would either be a contribution to the energy of the excitation from the Zeeman energy, which was positive and increasing as a function of field, or no contribution. In either case, the gap would be expected to grow faster with field in the high field (fully polarized) state than in the low field state but not not more slowly as reported in [49]. This is what was observed for the transition seen at $\nu = 8/5$ [54].

An alternative explanation of the results at $\nu = 2/3$, assumes a fully polarized ground state and identifies the change in slope at $B \approx 6.5$T with a change in the nature of the lowest lying excitations. For $B \gtrsim 6.5$T, the lowest energy excitations would be within the fully spin-polarized sector, while for $B \lesssim 6.5$T they would involve a spin-reversal. We can make a rough estimate of the energy of the spin-reversed excitation gap ignoring Landau level mixing (LLM) as follows. Previous estimates of the Coulomb energy of a spin-reversed quasiparticle energy put it at around 55% of the energy of the spin-polarized quasiparticle [9]. The Coulomb energy of a spin-reversed quasihole is unlikely to be much lower than that of the spin-polarized hole, while the additional Zeeman energy will make this excitation unfavorable. We therefore take for the value of the quasihole energy that of the spin-polarized hole. The results for this 'spin-reversed' energy gap are shown as a dashed line in Figure (15) and are seen to be quite close to the observed data points, although the difference between our results for the 'polarized' gap and the spin reversed' gap is small. Our estimate of the spin-reversed excitation applies both at $\nu = 1/3$ and $\nu = 2/3$ as we have neglected LLM, which allows electrons to make virtual transitions to other Landau levels and thereby screen the interaction in the lowest Landau level. These effects would be larger for systems at $\nu = 2/3$ than at $\nu = 1/3$ in the same magnetic field and could explain why the the spin-reversed excitation lies below the fully polarized excitation up to higher magnetic fields at $\nu = 2/3$ than at $\nu = 1/3$. A tilted field experiment [54] would be one method to determine whether our identification of the change of slope in the gap with field with a change in polarization of the lowest-lying excitation is correct.

The apparent absence of a significant reduction of the gap in the tetracene MIS structures ($\mu < 2.5 \times 10^5$ cm^2/Vs) on account of disorder, given its importance in the ultra-high mobility (12.8×10^6 cm^2/Vs) GaAs heterostructures, is puzzling. It suggests that the activated gap measured in transport measurements is affected by disorder in different ways in heterostructures and MIS structures. In the heterostructures, the disorder scattering is that of the ionized silicon donors which were in a layer about 800Å from the electrons [12]. In the MIS structures, on the other hand, the doping is controlled by a capacitance (~ 130 nFcm^{-2} [49]) with the backgate of order microns from the carriers. Here the disorder scattering is likely to be

that of neutral defects. It is possible that, in the heterostructures, the activation studies do not measure directly the energy to create a quasiparticle quasihole pair from the ground state, but rather the energy to excite quasiparticle (or quasiholes) out of bound states in the potential of the (charged) impurity distribution.

VIII. CONCLUSIONS

We have used diagonalizations of the Hamiltonians for finite size systems on a sphere to obtain estimates of the gaps at filling fractions in the Jain sequence $\nu = 1/3, 2/5, 3/7$ and 4/9 and at $\nu = 5/2$. We have emphasized how taking account properly of the systematic contributions to the excitation energy from the charge redistribution on the sphere in excited states is essential if one is to obtain accurate estimates of the gaps in the thermodynamic limit. Our results for the gaps are smaller than earlier estimates based on finite-size studies (for $\nu = 2/5$ and 3/7 [10]) and those based on the study of trial wavefunctions (for $\nu = 2/5, 3/7$ and 4/9 [19]). This difference is important, as estimates of the gap as a function of ν provide the most direct numerical estimates the effective mass of CF's [15, 17]. Our new results are consistent with the CF picture provided the logarithmic corrections to the effective mass are taken into account and are not well described by assuming a filling factor independent effective mass (see Fig 5).

We have shown that Gaussian and the z×Gaussian (zG) variational functions accurately describe subband wavefunctions and yield subband energies and lowest Landau level pseudopotentials, which are essentially indistinguishable from those obtained by solving for the subband wavefunctions exactly by direct numerical integration. These trial wavefunctions offer a significant improvement over the standard Fang-Howard (FH) form, which overestimates the standard deviation of the charge distribution, w, by as much as 50% depending on electron density, n_s, (see Fig 7). The lowest Landau level pseudopotentials, which are the starting point for the study of the fractional quantum Hall gaps, turn out to be accurately determined using any of the three trial forms (Gaussian, zG or FH) once w is known (see Fig 9). This offers a huge simplification over the previous *ab initio* approaches which used numerical integration to find the subband wavefunction and tables of pseudopotential parameters [22]. We have also computed the variation of the gaps at fractionally quantized Hall states as a function of width of the subband charge distribution. The results are parametrized in Eq 26 and Table II.

We have compared our computed gaps with measured activated gaps. We have found that, even after taking account of disorder broadening of states, the measured activation gaps in GaAs heterostructures are only around 60% of the computed gaps for the filling fractions $\nu = 1/3, 2/5, 3/7$ and 4/9 (see Table IV). This is to be contrasted with the activated gaps at $\nu = 1/3$ and 2/5 reported in tetracene MIS structures, which turn out to be reasonable agreement with computed gaps (see Fig 15). We have suggested that the relationship between the computed gap and the measured activated gap may be different depending on the type of disorder in the samples. In the GaAs heterostructures the charged donor ions, which are the main scattering centers, are only around 800Å from the quantum Hall layer, and this could lead to local variations in the energy required to excite quasiparticle-quasihole pairs with the lowest excitation energies controlling the activated transport. On the other hand, the backgate in the MIS structures is of order microns from the quantum Hall layer, and the main scattering centers are likely to be neutral. These are less likely to affect the energy to excite quasiparticle-quasihole pairs and the gap controlling activated transport should then be close to the true thermodynamic gap as we have found. For filling fractions $\nu = 2/3$ and $5/2$, the reported activated transport gaps in GaAs heterostructures are only around 10% and 5% respectively of the values we compute, although we have not attempted to account for disorder broadening in these cases. However, the experimental evidence suggests a disorder broadening which is comparable at $\nu = 5/2$ with the computed gap [48] so the large discrepancy is to be expected.

Acknowledgments

We would like to thank B.I. Halperin for helpful discussions. Two of us (RHM and SDS) would like to thank the ITP in Santa Barbara for its hospitality in 1998, which led directly to this project, and the Aspen Center for Physics for its hospitality in 2000 where this project made important progress.

Appendix: ZdS Interaction

One previous attempt to model finite width effects used the 'model interaction' [20]

$$V_{ZdS}(r) = \frac{e^2}{\varepsilon}\frac{1}{\sqrt{r^2+t^2}}, \tag{32}$$

which introduces a width parameter t. We have found that this model interaction cannot reproduce accurately the variation with L of the Haldane pseudopotential parameters for a sample with finite width with the errors significantly increasing as the width increases, Figure 16.

The reason for this is probably the unphysical nature of this interaction as a model for electrons in a heterostructure or quantum well interacting via the Coulomb interaction. Taking the Fourier transform of (14) and using the convolution theorem, one can show that it is not possible to construct a density distribution, $|\zeta(z)|^2$, for which the effective interaction (see14) is $V_{ZdS}(r)$. This is essentially because $V_{ZdS}(r)$ is the Coulomb interaction of two (distinguishable) particles confined to separate planes a distance t apart and, as such, misses the $\ln r$ found for small r and large widths for all realistic density distributions, $|\zeta(z)|^2$. However, many of the results obtained on the basis of the effective interaction are still valid if interpreted carefully.

For this purpose, we incorporate an overall scaling factor of the interaction N,

$$v_{ZdS}(r) = N\frac{e^2}{\varepsilon}\frac{1}{\sqrt{r^2+t^2}}, \tag{33}$$

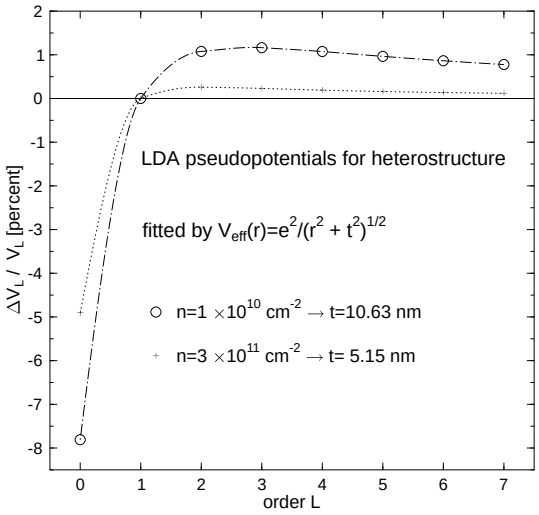

Figure 16: Errors in the Haldane pseudopotentials V_L computed using the Zhang-DasSarma model interaction (32). The comparison is with the values reported in [22]. The variational parameters are determined such that V_1 is correctly reproduced. Note in particular the large errors for V_0 and the slow decay of the error with increasing L for the low-density sample.

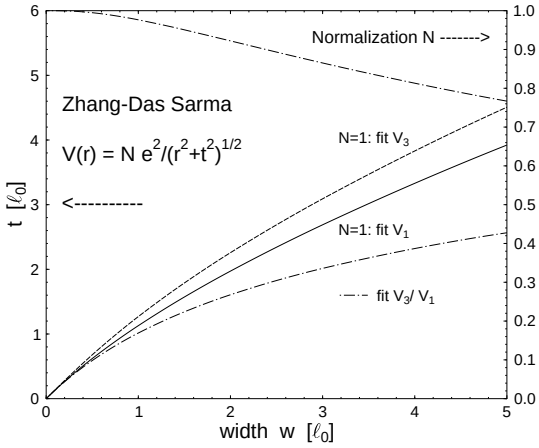

Figure 17: The width parameter t (lower three curves) in the ZDS model interaction in(33) and the normalization parameter N (top curve), as a function of the Gaussian width w of the density distribution, $\zeta(z)^2$. For the two curves labelled $N = 1$, the normalization is held equal to one and the parameter t is chosen so that the Haldane pseudopotential V_1(lower curve) and V_3 (upper curve) for the interaction in 33 are equal to the values obtained from (14) using the Gaussian variational wf's. The dashed-dotted curves show the values of t and N required to reproduce both V_1 and V_3/V_1 correctly.

with $N = 1$ giving the original interaction (32). The gap energies and relative stability of fractional quantum Hall states in the principal Jain sequence are determined principally by the first two Haldane pseudopotentials for odd angular momentum V_1 and V_3. In figure 17 we show the values of t required in 33 to match the values of V_1 and of V_3 to those obtained using the variational Gaussian wf as a function of the width parameter assuming $N = 1$. It is clear that it is not possible to find a value of t which gives both V_1 and V_3 correctly. If we allow N and t to vary then both V_1 and V_3 can be correctly reproduced by the effective interaction in (33). The results are also shown in Fig 17. Changing N means that the asymptotic behavior of the pseudopotentials at large angular momentum is not reproduced correctly. However, as the gaps and stability of the incompressible states in the Jain sequence are determined principally by the pseudopotentials $V_1$and V_3 this should not be a problem. If phase transitions between spin-singlet and polarized states (e.g. at $\nu = 2/5$) are of interest, it is obviously possible to correctly represent the in this case most important pseudopotentials V_1 and V_2 for angular momenta $L = 1$ and 2, by appropriate choice of N and t.

[1] D.C. Tsui, H.L. Störmer and A.C. Gossard, Phys Rev Lett **48**,1559(1982)
[2] R.B. Laughlin, Phys. Rev. Lett. **50,** 1395 (1983)
[3] F.D.M. Haldane, Phys. Rev. Lett. **51**, 605(1983)
[4] B.I. Halperin, Phys. Rev. Lett. **52,** 1583 (1984) and *ibid.* 2390(E)
[5] J.K. Jain, Phys. Rev. Lett. **63,** 199 (1989)
[6] F.D.M. Haldane and E.H. Rezayi, Phys. Rev. Lett. **54**, 237 (1985)
[7] G. Fano, F. Ortolani and E. Colombo, Phys. Rev. **B34**, 2670 (1986)
[8] R.H. Morf and B.I. Halperin, Phys. Rev. **B34**, 2670 (1986)
[9] R.H. Morf and B.I. Halperin, Z. Phys. **B68**, 391 (1987)
[10] N. d'Ambrumenil and R.Morf, Phys. Rev. **B40**, 6108, (1989)

[11] R.L. Willett, H.L. Störmer, D.C. Tsui, A.C. Gossard and J.H. English, Phys. Rev. **B37**, 8476 (1988)

[12] R.R. Du, H.L. Störmer, D.C. Tsui, L.N. Pfeiffer and K.W. West, Phys. Rev. Lett. **70**, 2944 (1993)

[13] R.R. Du, H.L. Störmer, D.C. Tsui, A.S. Yeh and K.W. West, Phys. Rev. Lett. **73**, 3274 (1994)

[14] G.S. Boebinger, A.M. Chang, H.L. Störmer and D.C. Tsui, Phys. Rev. Lett. **55**, 1606 (1985)

[15] B.I. Halperin, P.A. Lee and N. Read, Phys. Rev. **B47**, 7312 (1993)

[16] A. Stern and B.I. Halperin, Phys. Rev. B **52**, 5890 (1995)

[17] B.I. Halperin, Perspectives in Quantum Effects, p 225, ed S. das Sarma and A. Pinczuk, Wiley 1996

[18] R. Morf and N. d'Ambrumenil, Phys. Rev. Lett. **74**, 5116 (1995)

[19] J.K. Jain and R.K. Kamilla, Phys. Rev. B **55**, R4895 (1997)

[20] F.C. Zhang and S. Das Sarma, Phys. Rev. **B33**, 2903 (1986)

[21] D. Yoshioka, J. Phys. Soc. Jpn. **55**, 885 (1986); Surf Sci **170**, 125 (1986).

[22] M.W. Ortalano, S. He, and S. Das Sarma, Phys. Rev. **B55**, 7702 (1997)

[23] K. Park and J.K. Jain, Phys. Rev. Lett. **81**, 4200 (1998)

[24] R.H. Morf, Phys. Rev. Lett. **83**, 1485 (1999).

[25] K. Park and J.K. Jain, Phys. Rev. Lett. **83**, 1486 (1999) and K. Park, N. Meskini and J.K. Jain, J. Phys. Cond. Mat. **11**, 7283 (1999).

[26] D. Yoshioka, J. Phys. Soc. Jpn. **53**, 3740 (1984)

[27] X. Zhu and S.G. Louie, Phys. Rev. Lett. **70**, 339 (1993)

[28] B.I. Halperin, Helv. Phys. Acta **56**, 75 (1983)

[29] T. Chakraborty, P. Pietiläinen and F.C. Zhang, Phys. Rev. Lett. **57**, 130 (1986)

[30] E. Rezayi, Phys. Rev. **B43**, 5944 (1991)

[31] R.H. Morf, Phys. Rev. Lett. **80**, 1505 (1998)

[32] E.H. Rezayi and F.D.M. Haldane, Phys. Rev. Lett. **84**, 4685 (2000)

[33] M. Shayegan, J. Jo, Y.W. Suen, M. Santos and V.J. Goldman, Phys. Rev. Lett. **65**, 2916 (1990).

[34] Y.W. Suen, L.W. Engel, M.B. Santos, M. Shayegan and D.C. Tsui, Phys. Rev. Lett. **68**, 1379 (1992); J.P. Eisenstein, G.S. Boebinger, L.N. Pfeiffer, K.W. West and Song He, Phys. Rev. Lett. **68**, 1383 (1992)

[35] S. He, F.C. Zhang, X.C. Xie and S. Das Sarma, Phys. Rev. **B42**, 11376 (1990)

[36] F. Stern and S. Das Sarma, Phys. Rev. **B30**, 840 (1984)

[37] T. Ando, A.B. Fowler and F. Stern, Rev. Mod. Phys. **54**, 437 (1982)

[38] F.D.M. Haldane in The Quantum Hall Effect, ed. by R.E. Prange and S.M. Girvin (Spinger-Verlag, New York, 1987)

[39] X. G. Wen and A. Zee, Phys. Rev. Lett. **69**, 953 (1992); ibid **69**, 3000 (1992)

[40] G. Fano and F. Ortolani, Phys. Rev B **37**, 8179 (1988)

[41] B. Jancovici, Phys. Rev. Lett. **46**, 386 (1981)

[42] R.L. Willett, J.P. Eisenstein, H.L. Störmer, D.C. Tsui, A.C. Gossard and J.H. English, Phys. Rev. Lett. **59**, 1776 (1987)

[43] G. Murthy and R. Shankar, Phys. Rev. B **59**, 12260 (1999).

[44] R. Shankar and G. Murthy, Phys. Rev. Lett **79**, 4437 (1997); R. Shankar, Phys. Rev. Lett. **83**, 2382 (1999); R. Shankar, Phys. Rev. B **63**, 085322 (2001) and Erratum: Phys. Rev. B **64**, 049902 (2001)

[45] G. Moore and N. Read, Nucl Phys B **360,** 362 (1991)

[46] J.P. Eisenstein, K.B. Cooper, L.N. Pfeiffer and K.W. West, Phys. Rev. Lett. **88**, 076801-1 (2002)

[47] J.P. Eisenstein, R.L. Willett, H.L. Stormer, L.N. Pfeiffer, K.W. West, Surface Science **229**, 31 (1990)

[48] W. Pan, Xia JS, Shvarts V, Adams DE, Stormer HL, Tsui DC, Pfeiffer LN, Baldwin KW, West KW, Phys. Rev. Lett. **83**, 3530 (1999)

[49] J.H. Schön, Ch. Kloc and B. Batlogg, J. Phys: Cond. Matt. **13**, L163 (2001); Science **288**, 2338 (2000).

[50] E.H. Rezayi and F.D.M. Haldane, Phys. Rev. B**42**, 4532 (1990)

[51] E.H. Rezayi, Phys. Rev. B**43**, 5944 (1991)

[52] J.D. Jackson, Classical Electrodynamics (3rd edition, p 154), Wiley (1999).

[53] The results for the theoretical values of the energy gaps at $\nu = 1/3$ and 2/5 reported in Reference [49] are apparently based on different values of the dielectric constant, $\epsilon = 5.86$ at $\nu = 1/3$ and $\epsilon = 6.6$ at $\nu = 2/5$. This is not discussed in Reference [49].

[54] J.P. Eisenstein, H.L. Störmer, L.N. Pfeiffer and K.W. West, Phys. Rev. Lett **62**, 1540 (1990); J.P. Eisenstein in *Perspectives in Quantum Hall Effects*, edited S. das Sarma and A. Pinczuk (Wiley 1997).

[55] N. Freytag, Y. Tokunaga, M. Horvatic, C. Berthier, M. Shayegan and L.P. Levy, Phys. Rev. Lett **87**, 136801 (2001).